การผลิตอนุภาคคาร์บอนระดับนาโนเมตรโดยใช้วิธีการปล่อยอาร์คไฟฟ้าในน้ำ

นาย ปุลศักดิ์ มุทธากาญจน์

วิทยานิพนธ์นี้เป็นส่วนหนึ่งของการศึกษาตามหลักสูตรปริญญาวิศวกรรมศาสตรมหาบัณฑิต
สาขาวิชาวิศวกรรมเคมี ภาควิชาวิศวกรรมเคมี
คณะวิศวกรรมศาสตร์ จุฬาลงกรณ์มหาวิทยาลัย
ปีการศึกษา 2547
ISBN 974-53-1309-2

PRODUCTION OF CARBON NANOPARTICLES USING ARC DISCHARGE IN WATER METHOD

Mr. Poonlasak Muthakarn

A Thesis Submitted in Partial Fulfillment of the Requirements
for the Degree of Master of Engineering in Chemical Engineering
Department of Chemical Engineering
Faculty of Engineering
Chulalongkorn University
Academic Year 2004
ISBN 974-53-1309-2

Thesis Title	PRODUCTION OF CARBON NANOPARTICLES USING ARC DISCHARGE IN WATER METHOD
By	Mr. Poonlasak Muthakarn
Field of study	Chemical Engineering
Thesis Advisor	Associate Professor Tawatchai Charinpanitkul, D.Eng.
Thesis Co-advisor	Professor Wiwut Tanthapanichakoon, Ph.D.

Accepted by the Faculty of Engineering, Chulalongkorn University in Partial Fulfillment of the Requirements for the Master's Degree

……Dean of the Faculty of Engineering
(Professor Direk Lavansiri, Ph.D.)

THESIS COMMITTEE

……Chairman
(Associate Professor Suttichai Assabumrungrat, Ph.D.)

……Thesis Advisor
(Associate Professor Tawatchai Charinpanitkul, D.Eng.)

…… Thesis Co-advisor
(Professor Wiwut Tanthapanichakoon, Ph.D.)

…… Member
(Nattaporn Tonanon, M.Sc.)

…… Member
(Varong Pavarajarn, Ph.D.)

ปุลศักดิ์ มุทธากาญจน์ : การผลิตอนุภาคคาร์บอนระดับนาโนเมตรโดยใช้วิธีการปล่อยอาร์คไฟฟ้าในน้ำ (PRODUCTION OF CARBON NANOPARTICLES USING ARC DISCHARGE IN WATER METHOD) อ. ที่ปรึกษา : รศ. ดร.ธวัชชัย ชรินพาณิชกุล, อ. ที่ปรึกษาร่วม : ศ. ดร. วิวัฒน์ ตัณฑะพานิชกุล จำนวนหน้า 116 หน้า. ISBN 974-53-1309-2.

การปล่อยอาร์คไฟฟ้าในของเหลวเป็นวิธีใหม่ที่ถูกพัฒนาขึ้นเพื่อใช้ในการผลิตอนุภาคคาร์บอนระดับนาโนเมตรโดยมีต้นทุนที่ต่ำกว่าวิธีอื่น ในงานนี้ได้มีการศึกษาถึงผลของของเหลวอินทรีย์เช่น แอลกอฮอล์ ($C_mH_{2m+1}OH$, m=1-8) อัลเคน (C_mH_{2m+2}, m=6-7) และสารประกอบอะโรแมติก (C_6H_6-C_nH_{2n}, n=1-2) รวมทั้งผลของสารละลายเกลืออนินทรีย์ อาทิเช่น Na_2CO_3, $NiSO_4$, $CoSO_4$ และ $FeSO_4$ ที่มีต่อโครงสร้างและค่าผลได้ของผลิตภัณฑ์ที่มีอนุภาคนาโนคาร์บอนปนอยู่ในปริมาณที่สูง จากการศึกษาพบว่าท่อนาโนคาร์บอนแบบผนังหลายชั้นและอนุภาคพอลิฮิดรอลสามารถสังเคราะห์ได้ในความเข้มข้นสูง โดยอนุภาคที่ได้จะเกาะอยู่ที่ปลายขั้วคาโทด เมื่อของเหลวอินทรีย์ถูกใช้ในการอาร์ค ไม่เพียงแต่แท่งกราไฟต์อิเล็กโทรดเท่านั้นที่ช่วยจ่ายคาร์บอนให้กับระบบ แต่ของเหลวอินทรีย์เหล่านี้ยังสามารถเป็นแหล่งคาร์บอนได้อีกทางหนึ่ง ซึ่งสามารถช่วยเพิ่มค่าผลได้มากกว่า 8 -100 เท่าเมื่อเทียบกับการปล่อยอาร์คไฟฟ้าในน้ำ

ในกรณีของสารละลายเกลืออนินทรีย์ การใช้ไอออนผสมเข้าไปในบริเวณที่เกิดปฏิกิริยาในปริมาณระหว่าง 0.01 ถึง 0.05 M สามารถช่วยเป็นตัวเร่งปฏิกิริยาทำให้การเกิดของอนุภาคนาโนคาร์บอนดีขึ้น นอกจากนี้ชนิดของสารประกอบโลหะผลพลอยได้ที่มีรูปร่างแบบต่างๆ นั้นสามารถสังเคราะห์ได้โดยการปรับความเข้มข้นของสารละลายเกลือที่ใช้

นอกจากนี้เมื่อใช้สารลดแรงตึงผิว (monoolein) ในการเตรียมสารละลายผสมระหว่างของเหลวอินทรีย์และน้ำเพื่อใช้เป็นของเหลวสำหรับการอาร์ค จากการศึกษาพบว่าความดันไอของเฮกเซนลดลงประมาณ 1500 ถึง 10000 เท่า เมื่อเทียบกับกรณีเฮกเซนบริสุทธิ์ ซึ่งเทคนิคนี้เป็นทางเลือกใหม่ ในการเพิ่มคาร์บอนในระบบไปยังบริเวณที่เกิดปฏิกิริยาโดยมีความปลอดภัยกว่าการใช้สารอินทรีย์บริสุทธิ์ซึ่งมีความดันไอของของเหลวสูง

ภาควิชา วิศวกรรมเคมี ลายมือชื่อนิสิต.....

สาขาวิชา วิศวกรรมเคมี ลายมือชื่ออาจารย์ที่ปรึกษา.....

ปีการศึกษา 2547 ลายมือชื่ออาจารย์ที่ปรึกษาร่วม.....

4570423921: MAJOR ENGINEERING

KEY WORD: CARBON NANOPARTICLES / ARC DISCHARGE / SEM&TEM ANALYSIS / MWCNTs

POONLASAK MUTHAKARN: PRODUCTION OF CARBON NANOPARTILCES USING ARC DISCHARGE IN WATER METHOD. THESIS ADVISOR: ASSOC. PROF. TAWATCHAI CHARINPANITKUL, D.Eng., THESIS CO-ADVISOR : PROF. WIWUT TANTHAPANICHAKOON, Ph.D., 116 pp. ISBN 974-53-1309-2

'Arc in liquid' method has been recently developed as a low-cost technique to fabricate carbon nanostructures. In this work, the effects of organic liquid such as alcohols ($C_mH_{2m+1}OH$, m=1-8), alkanes (C_mH_{2m+2}, m=6-7), and aromatic compounds (C_6H_6-C_nH_{2n}, n=1-2) as well as inorganic salt solution such as Na_2CO_3, $NiSO_4$, $CoSO_4$ and $FeSO_4$ on the product structures and yield of nanocarbon-rich deposits were investigated. Multi-walled carbon nanotubes (MW-CNTs) and polyhedral nanoparticles were successfully produced with high concentration as the hard deposit formed at the cathode tip in all condition. When organic compounds were applied as liquid media, not only graphite electrodes but also organic liquid compounds as an additional carbon source to produce carbon nanoparticles which lead to approximately 8-100 times higher yield than the 'arc in water' system.

For inorganic salt solution system, the existence of ions, even only a little amount (0.01-0.05 M), in reaction zone could play an important role as a catalyst to enhance the formation rate of CNPs. Additionally, metallic byproduct compounds with various shapes depending on the aqueous concentration could be found in the synthesized products.

By using surfactant (monoolein) to prepare the organic liquid-water mixture to accommodate the arc, n-hexane of which vapor pressure is 1,500-10,000 times lower than pure n-hexane compound, could be obtained. This is an effectively alternative method to provide more carbon atoms for reaction which could provide higher safety than using pure organic liquid.

Department Chemical Engineering Student's signature..... .....

Field of study Chemical Engineering Advisor's signature.....

Academic year 2004 Co-advisor's signature.....

ACKNOWLEDGEMENT

Firstly, I sincerely wish to thank Assoc. Prof. T. Charinpanitkul, thesis advisor, and Prof. W. Tanthapanichakoon, thesis co-advisor, for their introducing this interesting project with the indispensable advice and warmest encouragement. In addition, I am also grateful to Assoc. Prof. N. Sano of University of Hyogo for his on-the-job training, useful guidance, research assistant, deep discussion and kindness during my one-year research in University of Hyogo, Japan. Moreover, I am very grateful to Assoc. Prof. S. Assabumrungrat, Ms. N. Tonanon, and Dr. V. Pavarajarn for their simulative comments and participation as my thesis committee.

Next, I would like to acknowledge Ministry of University Affairs, Thailand Research Fund (TRF), University-Industry Collaborative Research Project and Rachadapisek Sompoch Fund of Chulalongkorn University, and technical support from National Science and Technology Development Agency (NSTDA). I would like to thank Association of International Education Japan (AIEJ) for the scholarship to study and do research at University of Hyogo, Japan (2004-2005).

This research received research grant from the University-Industry collaborative project (Production of Carbon Nanoparticles using Arc Discharge in Water Project). Prof. Wiwut heads the project and I am one of the full-time research assistants. In addition, this project also received the grant from Grant-in-Aid for Young Scientists (B) of Japan Society for the Promotion of Science (JSPS) (No.14750618)

I would like to thank Prof. T. Kanki, University of Hyogo, for his valuable suggestion and kindness. He passed away during my one-year research in Japan. I pray for his peaceful eternal rest and a blissful afterlife.

Moreover, I would like to thank Dept. of Chemical Engineering, Chulalongkorn University and Dept. of Mechanical and System Engineering, University of Hyogo for allowing me to setup the experimental apparatus and using the valuable accessories.

Furthermore, I would like to acknowledge the hospitality and encouragement of all members in PTMP Laboratory, Chulalongkorn University, and Transport phenomena Laboratory, University of Hyogo during my short-visit in Japan

Eventually, I would like to express the appreciation to my parents for their supports and understandings in my life throughout the course of education.

CONTENTS

CHAPTER Page

CHAPTER Page

CHAPTER Page

CHAPTER Page

CHAPTER Page

LIST OF TABLES

LIST OF FIGURES

Page

Page

Page

Page

Page

NOMENCLATURES

MW-CNTs, MWNTs	Multi-walled carbon nanotubes
SW-CNTs, SWNTs	Single-walled carbon nanotubes
DW-CNTs	Double-walled carbon nanotubes
CNPs	Carbon nanoparticles
SEM	Scanning Electron Microscope
TEM	Transmission Electron Microscope
XRD	X-ray diffraction
HRTEM	High Resolution Transmission Electron Microscope
DLS	Dynamic Light Scattering
RBM	Radial Breathing Mode
CNTs	Carbon nanotubes
SWNHs	Single-walled nanohorns
DC	Direct Current
AC	Alternating Current
EDX	Energy Dispersive X-Ray

CHAPTER I

INTRODUCTION

1.1 Background

Nowadays, fabrication, characterization and application of carbon nanoparticles have been widely studied since fullerenes and multi-walled carbon nanotubes (MW-CNTs) were discovered, i.e., single-walled carbon nanotubes (SW-CNTs), double-walled carbon nanotubes (DW-CNTs), carbon nanohorns, carbon nano onions and metal-filled carbon nanocapsules. It is believed that these nano materials have potential to use for various industrial applications [1] including gas storage components (argon, nitrogen, and hydrogen), field emission devices, reinforced composite materials, high power electrochemical capacitors, electronic nanoswitches, chemical sensors, magnetic data storage, and high quality lubricants.

Various fabrication techniques have been proposed [1], for example, laser ablation, thermal pyrolysis of gas species, plasma-enhanced chemical vapor deposition, electrolysis and arc discharge in reduced-pressure gases. However, such synthesis techniques have still been facing with some difficulties because of the high cost of investment and operation. Under this circumstance, it is demanded to develop cost-effective fabrication methods. Recently, a new method using arc discharge submerged in water was proposed [2]. This method is outstanding in a point that it does not require inert gas and vacuum system so that the setting cost is extremely low

and produces uncontaminated. Moreover, this method can produce not only carbon nanoparticles but also other nanostructures, inorganic fullerenes and polyynes.

In the reported conditions of ‘arc in liquid’ method, when water or liquid nitrogen is used as liquid media, carbon nanoparticles (CNPs) including MW-CNTs and nano onions were produced from carbon vapor which was supplied from a graphite electrode as a carbon source, and the liquid played a role as quenching media to cool down the carbon vapor in the gas bubble to form various nanostructures. So far, some important parameters of this reaction field have been investigated, such as, current density [2], gas pressure [3], and liquid flow [4]. However, gas components in bubbles at the arc plasma are also important factor which has not been clarified. One possible way to increase carbon vapor in the gas bubble is to provide additional carbon source into arc discharge system beside graphite electrodes. Such modified conditions may increase the synthesized CNPs to help the scale-up of this process because the production of CNPs is limited by the evaporation rate of graphite electrodes in the conventional arc-in-water condition. For this expectation, liquid components which have carbon atoms in their molecules such as alcohols, alkanes, aromatic compounds, and sodium carbonate solution (Na_2CO_3) were used as quenching media. Moreover, surfactant was also employed to mix the water and organic compound for producing the colloid liquid which contained high amount of organic compound in the water, leading to increase the carbon source in the liquid media also. Another possible way to increase yield and production rate of CNPs is to add the inorganic catalyst such as Ni, Co, and Fe into liquid media to enhance self assembly reactions. This work will describe the effect of these compounds on the yield and production rate of the synthesized CNPs.

1.2 Objective of Study

To produce nanoparticles using arc discharge in water and to investigate the effect of organic and inorganic species existing in liquid media on the structures and yield of nanoparticles.

1.3 Scope of Study

1.3.1 Design and construct the experimental apparatus

1.3.2 Study the effect of organic and inorganic species at current 50 A

1.3.2.1 Species of organic components to be investigate

- Use of alcohol-water mixtures (methanol & ethanol)
- Use of alcohol ($C_mH_{2m+1}OH$, m=1-8)
- Use of alkane (C_mH_{2m+2}, m=6-7)
- Use of aromatic compounds (C_6H_6-C_nH_{2n}, n=1-2)
- Use of a suitable surfactant (Monoolein, $C_{17}H_{35}COO$-$CH_2CH(OH)CH_2OH$)

1.3.2.2 Species of inorganic aqueous solution to be investigate

- Use of sodium carbonate solution (Na_2CO_3)
- Use of transition metal salt solutions ($NiSO_4$, $CoSO_4$, $FeSO_4$)

1.3.3 Characterize the obtained nanoparticles using SEM (Scanning Electron Microscopy), TEM (Transmission Electron Microscopy), XRD (X-ray diffraction) and Raman Spectroscopy

1.4 Procedure of the research

1.4.1 Explore and review the related researches

1.4.2 Design and construct the experimental setup

1.4.3 Conduct experiments to repeat the conventional method of nanoparticles-synthesis

1.4.4 Conduct experiments by varying electricity current, species of the organic and inorganic liquid

1.4.5 Study and estimate properties of the obtained nanoparticles

1.4.6 Discuss experimental results

1.4.7 Draw conclusion

1.4.8 Write the thesis

1.5 Obtained Benefits

1.5.1 Knowledge of arc discharge mechanism will be obtained

1.5.2 Understanding in the effect of type of liquids and additives on the observed nanostructures and yield of nanoparticles

1.5.3 Knowledge of arc discharge method should be adaptable for mass production of nanoparticles

CHAPTER II

LITERATURE REVIEW

2.1 Synthesis of nanoparticles by arc discharge in liquids method

N. Sano, H. Wang, I. Alexandron et al. [2] used an arc discharge method to fabricate high-quality nanoparticles including spherical carbon onions and elongated fullerene-like nanoparticles similar to nanotubes in large quantities without the use of vacuum equipment. The nanoparticles were obtained in the form of floating powder on the water. HRTEM and SEM results showed the presence of spherical carbon onions with diameters ranging from 4 to 36 nm. The specific surface area of the obtained particles was as large as 984.3 m^3/g. They also proposed the mechanism to explain the formation of the carbon onions. Moreover, they offered that the physical characteristics of the product can be controlled by manipulating voltage of electricity supplied to the electrodes

N. Sano, M. Naito, M. Chhowalla et al. [3] synthesized of multi-walled carbon nanotubes (MW-CNTs) by an arc discharge between two graphite electrodes submerged in water under controlled pressure (from 400 to 760 Torr). They found that product collected from the bottom of the reactor revealed high concentrations of MW-CNTs regardless of pressures. Dynamic light scattering (DLS) on suspensions containing MW-CNTs showed that the mean diameter of the nanotubes increases with decreasing pressure. Raman spectroscopy analysis revealed that the relative amount of

disordered carbon was significantly less in the low-pressure samples. Furthermore, the yield of the deposit was found to be independent of the pressure. They concluded that the physical properties of MW-CNTs formed by the submerged arc can be controlled by manipulating the pressure.

N. Sano, T. Charinpanitkul, T. Kanki, and W. Tanthapanichakoon [4] investigated the effect of force convection jet on the arc plasma to synthesize CNPs such as MW-CNTs and multi-shelled nanoparticles by 'arc in water' method. They found that there is an optimized flow rate of the convective jet that leads to the highest yield, largest hydrodynamic diameter of the products, and the reduced crystalline defects. With the convection flow rate of 1.36 dm^3 /min, the highest yield and production rate of CNPs could be obtained at 48.5% and 9.32 g/h, respectively.

H.W. Zhu, X.S. Li, B. Jiang et al. [5] used an arc in water method for growing carbon nanotubes. They found that carbon nanotubes (CNTs) with highest purity (20%) and highest yield (7 mg/min.) were obtained when using salt solution ($NiSO_4$, $CoSO_4$ and $FeSO_4$) as the medium. The data from Resonance Raman spectrum of multiwalled carbon nanotubes (MW-CNTs) and RBM peaks revealed that high-quality MW-CNTs can be effectively prepared in water-arcing process.

N. Sano, H. Wang, M. Chhowalla et al. [6] used an arc discharge between a graphite cathode and a molybdenum anode filled with molybdenum disulfide (MoS_2) powder submerged in de-ionized water to produce closed caged fullerene-like MoS_2 nano-particles. They investigated a statistical study of over 150 polyhedral fullerene-

like MoS_2 nano-particles in plan view and transmission electron microscopy revealed that the majority consisted of 2-3 layers with diameters of 5-15 nm. They showed that the nano-particles are formed by seamless folding of MoS_2 sheets and model based on the agglomeration of MoS_2 fragments over an extreme temperature gradient around a plasma ball in water was also proposed to explain the formation of nano-particles.

X. Li, H. Zhu, B. Jiang et al. [7] used a water-protected arc discharge (WPAD) method by using a graphite cover to produce CNTs on large scale. They could synthesize CNTs with a higher production rate and yield than the conventional arc in water method, because the graphite cover would help to protect the side-reaction between carbon and water.

S. Cui, P. Scharff, C. Siegmund et al. [8] synthesized multi-walled carbon nanotubes (MW-CNTs) using submerged arc in liquid nitrogen. The anode was the mixture of Fe_2O_3, Co_2O_3, NiO and graphite powder. Each of the Fe, Co, and Ni elements was 1.5 weight % in the graphite powder. The cost of MW-CNTs produced by this method could be reduced remarkably hereby, and the safety was obviously increased, compared to helium or H_2 atmospheres.

H. Lange, M. Sioda, A. Huczko et al. [9] synthesized carbon nanostructures (onions, nanotubes and encapsulates) by arc discharge in water between pure and catalyst-doped graphite electrodes. These carbon structures were of fine quality and crystalline morphology, similar to those formed in He arc plasma. Emission spectroscopy was performed to assess the plasma components (H, O, C and C_2) and

temperature values. C_2 radicals were determined quantitatively, between 10^{15}- 10^{16} cm^{-2} depending on graphite anode composition and the temperature of plasma was between 4000 and 6500 K.

M. V. Antisari, R. Marazzi, and R. Krsmanovic [10] synthesized multi-walled carbon nanotubes (MW-CNTs) by an electric arc discharge performed in liquid environments between pure graphite electrodes. They found that both of nitrogen and deionized water were suitable for a successful synthesis of this form of carbon aggregation. Electron microscopy observations of both the reaction products and the surface of the as-synthesized raw material showed the presence of structural degradation of the MW-CNTs. The degradation is tentatively ascribed to a combination of overheating and high current density experience by the as-synthesized MW-CNTs. The damage appeared to be less severe in water environments, probably owing to the better cooling capacity of water relative to liquid nitrogen.

L. P. Biro, Z. E. Horvarth, L. Szalmas et al. [11] produced multi-walled carbon nanotubes by an AC arc in water between two carbon electrodes. They reported that at a voltage of 40 V, the arc is stable in the range of 85-45 A, and lower current values help in increasing the fraction of carbon nanotubes in the products.

N. Sano [12] used benzene (C_6H_6) as a liquid media. He found multi-shelled nanoparticles of diameter 10-30 nm in the deposits formed between electrodes, in which highly curled graphitic structure are majority product. Moreover, he also found

that CNTs and fullerene was not produced in this condition, which is different from arc in water or liquid nitrogen.

N. Sano [13] used arc discharge in water with N_2 injection into the arc plasma to produce single-walled carbon nanohorns (SWNHs). Arc plasma between the graphite electrodes was isolated from the surrounding water by a thin graphite wall with an N_2 flow that excluded reactive gas species (H_2O, CO and H_2) from arc zone. He found the high concentration of SWNHs as fine powder floating on the water surface. The particle size distribution of SWNHs was evaluated by dynamic light scattering, resulting in an approximately 70 nm peak diameter.

N. Sano, J. Nakano, and T. Kanki [14] reported the synthesis of single-wall carbon nanotubes and nanohorns by arc in liquid nitrogen with composite electrodes consisting of graphite mixed with Ni. They found that the moderate concentration of Ni in the composite anode (1.8-4.6 mol %) and the relatively inert environment at the arc zone are important factors for producing the SWCNTs-SWNHs mixture.

N. Sano [15] synthesized Gd-included SWNHs and SWNTs by gas-injected ‘arc in water’ method, in which arc discharge was generated between a hollow graphite cathode and a metal-doped anode with N_2 gas injection. He proposed that this technique realized a new low-cost route to produce metal-hybridized single-wall particles. The Gd-included SWNHs with catalytic-grown SWNTs were collected as the floating powders in his process. Raman analysis on the floating products showed

that the crystallinity depends on the electrodes' dimensions. In the sedimentary deposit, Gd-stuffed MWNTs and multi-shelled CNPs were produced.

.

L. A. Montoro, R. C. Z. Lofrano, and J. M. Rosolen [16] reported the synthesis of high-quality SWNTs and MWNTs through arc-discharge in H_3VO_4 aqueous solution from pure graphite electrodes.

M. T. Beck, Z. Dinya, and S. Keki [17] used the DC electric arc in toluene with one or both electrodes being graphite. They found that there is the formation of a great number of polycyclic aromatic compounds up to 604 mass numbers in the residual liquid.

M. T. Beck, Z. Dinya, S. Keki, and L. Papp [18] continued their experiment by using high voltage (20 kV) with the electric discharges in liquid toluene between graphite or pyrographite electrodes. They found that C_{60} fullerene was also formed besides a great number of polycyclic aromatic hydrocarbons.

2.2 Synthesis of nanoparticles by arc discharge in gas environments

X. Zhao, M. Ohkohchi, M. Wang et al. [19] prepared fine and long multi-walled carbon nanotubes attached with less carbon nanoparticles by DC arc discharge of graphite electrodes in hydrogen gas. These high-grade carbon nanotubes grew on the central part of the cathode as a carbon deposit like black soot. A new type of carbon allotrope, namely petal-like graphite sheets consisting of a number of

interlaced graphene sheets, was also found in the outside region surrounding the central cathode deposit.

H. Zeng, L. Zhu, G. Hao and R. Sheng [20] used AC arc discharge method with He at low pressure to produce carbon nanoparticles. They found carbon nanocapsule, carbon cone-shaped nanotube and the toroidal nanotube in the soot (but not the cathode deposit). They also discussed the difference of formation mechanisms between AC and DC arc discharge.

J. L. Hutchison, N. A. Kiselev, E. P. Krinichnaya et al. [21] synthesized DW-CNTs by using arc discharge in Ar and H_2 mixture (1:1/v:v) at 350 Torr with catalyst which was prepared from a mixture of Ni, Co, Fe and S powders heated in an inert gas atmosphere at 500 C for 1 hr. They found DW-CNTs with outer diameter in the range of 1.9-5 nm and inner diameter in the range 1.1-4.2 nm and these DW-CNTs formed into bundles.

M. Cadek, R. Murphy, B. McCarthy et al. [22] studied the effect of varying current density and pressure during arc generation on the yield and purity of multi-walled nanotube-containing carbon soot. Various soots were produced and characterised qualitatively using transmission electron microscopy and quantitatively using electron paramagnetic resonance and thermogravimetric analysis. They found that both yield and purity increase as current density and pressure are increased to the limit of their experimental investigation (195 A/cm^2 and 500 Torr of helium). From

these conditions a yield of 24 mg/min. soot containing 48% by mass nanotubes was obtained.

Y. Wang, Z. Zhang, H. Liu et al. [23] synthesized single-walled carbon nanotubes (SWNTs) by arc discharge in He environment with a mixture of nickel and yttrium as catalysts. Their results indicate that the diameter distribution of SWNTs is in the range of 1.2-1.6 nm, and the SWNTs with diameter 1.43 nm are in the majority. The catalyst concentrations have large effect on the yield of SWNTs and little effect on the diameter distribution of SWNTs.

Y. Ando, X. Zhao, S. Inoue, and S. Iijima [24] studied that highly graphitized multiwalled carbon nanotubes (MW-CNTs) were mass-produced by hydrogen arc discharge with automatic feeding of carbon electrode. After collecting the products, MW-CNTs were purified by refluxing them in hydrogen peroxide and then in a mixture of sulfuric and nitric acids, respectively. They found that the purified MW-CNTs had about 1.3 nm innermost diameters.

M. Nishio, S. Akita, and Y. Nakayama [25] studied the cooling effect of the arc plasma region in He gas. They found that the yield of carbon nanotubes strongly depends on the cooling rate. In addition, nanotubes were grown on both the anode and the cathode. The optical emission spectra from the arc plasma indicate that the plasma temperature increases at the optimum cooling rate.

.

2.3 Characterization and properties of carbon nanoparticles

Y. Ando, X. Zhao, H. shimoyama et al. [26] studied some physical properties of MW-CNTs which were prepared by hydrogen arc discharge and were purified by using an infrared radiation heating system. They found that the purified MW-CNTs had a high degree of graphitization, an electrical conductivity of about 1.85 $x10^3$ Scm^{-1} along the long axis, and an enormous current density of more than 10^7 Acm^{-2}.

X. Zhao, Y. Ando, L. C. Qin et al. [27] studied the characteristic of MW-CNTs which were prepared by hydrogen arc discharge. These MW-CNTs were analyzed by using micro, polarized, resonance and surface-enhanced Raman scattering techniques. They can estimate the inner diameter of MW-CNTs from RBMs mode, resulting that the core nanotube with the smallest diameter of 0.4 nm were found. The multiple splitting of graphite-like G mode of MW-CNTs as also found in the surface-enhanced Raman spectra of isolated MW-CNTs.

CHAPTER III

THEORY

3.1 Carbon nanoparticles (CNPs)

Generally, it is known that carbon nanostructures which could be obtained from arc discharge method are fullerene, carbon nanotubes (CNTs), carbon nano onions, carbon nanocapsules, multi-shelled carbon nanoparticles, and carbon nanohorns (CNHs). Among these, carbon nanotubes have gained much more attention due to its prospective characteristics.

3.1.1 C_{60}: Buckminsterfullerene [1]

For several centuries, it was believed that only allotropes of carbon were graphite and diamond. However, in 1985, a new form of carbon, C_{60}: Buckminsterfullerene, was first produced and identified by H. W. Kroto. The structure of C_{60} fullerene is shown in Fig. 3.1.

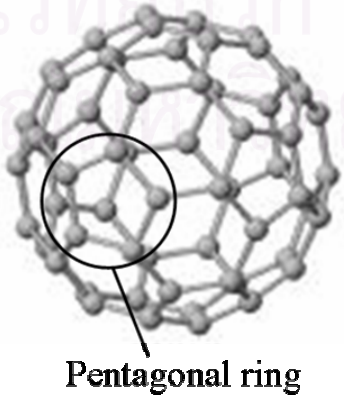

Figure 3.1 C_{60} Buckminsterfullerene [28]

The C_{60} molecule contains 60 atoms arranged in a spherical way, as in a soccer ball (truncated icosahedron). In C_{60}, sp^2 hybridized carbon (as in graphite) is curved by the introduction of pentagonal rings as also shown in Fig. 3.1.

3.1.2 Carbon nanotubes (CNTs) [1]

Carbon nanotubes can be considered as elongated fullerene. In 1991, S. Iijima published the structure of these systems consisting of concentric graphene cylinders (multi-walled carbon nanotubes: MW-CNTs), produced in the Kratschmer-Huffman fullerene reactor (operating at low direct current). Interestingly, these nested tubes exhibited interlayer spacing of 3.4 A^o, a value that is slightly greater than that of graphite (3.35 A^o). Iijima attributed this difference to a combination of the tubule curvature and van der Waals interactions between the successive cylinders. Two types of CNTs can be categorized if considering the types of CNTs wall. One is single-walled carbon nanotubes (SWCNTs). Another is multi-walled carbon nanotubes (MWCNTs). These structures are shown in Fig. 3.2.

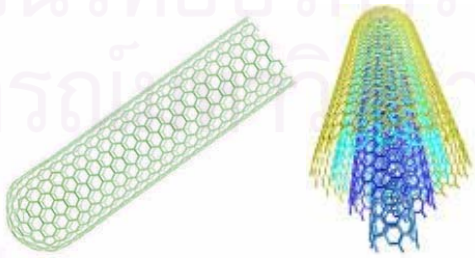

Figure 3.2 Carbon nanotube (CNTs) structure, single-walled carbon nanotube (SW-CNTs) (left), and multi-walled carbon nanotube (MW-CNTs) (right) [29]

Structure of carbon nanotubes from carbon atoms arrangement [1]

Theoretically, it is possible to construct a carbon tubule by rolling up a hexagonal graphene sheet in various ways. Two of these are ‘non-chiral’, so that the honeycomb lattices located at the top and bottom of the tube are always parallel. These configurations are known as ‘armchair’ and ‘zigzag’. In the armchair structure, two C-C bonds on opposite sides of each hexagon are perpendicular to the tube axis, whereas, in the zigzag arrangement, these bonds are parallel to the tube axis (Fig. 3.3a-b). All other conformations, where the C-C bonds lie at an angle to the tube axis, are known as ‘chiral’ or helical structures (Fig. 3.3c).

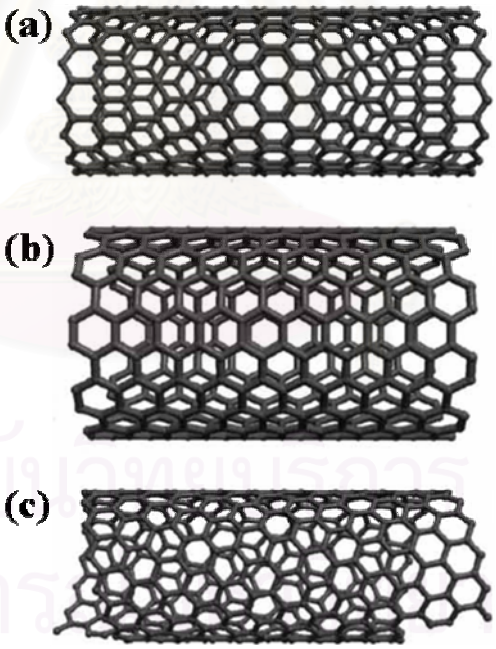

Figure 3.3 Molecular models SWNTs exhibiting different chiralities.

(a) zigzag arrangement; (b) armchair configuration;

(c) chiral conformation [1]

At present, carbon nanotubes can be obtained using various techniques: arc discharge, pyrolysis of hydrocarbons over catalysts, laser and solar vaporization, and electrolysis. These nanoscale materials can exhibit different morphologies such as straight, curled, hemitoroidal, branched, spiral, helix-shaped, etc.

In 1992, two groups predicted theoretically that single-walled carbon nanotubes (SWCNTs) might be metallic or semiconducting carbon nanowires, depending upon their helicity and diameter. These results amazed the community because bulk graphite can only behave as semimetal. In the mid and late 1990s, various groups conducted transport measurements on bulk MWCNTs, individual multilayered tubes, and ropes of SWCNTs. These reports revealed that the conducting properties of tubes indeed depend on the degree of graphitization, chirality, and diameter. Subsequently, Young's modulus measurements demonstrated that multilayered carbon nanotubes are mechanically much stronger than conventional carbon fibres and are extraordinarity flexible when subjected to large strain.

3.1.3 Carbon nano onion [29]

Carbon nano onion has a central shell about 0.7-1 nm in diameter, i.e. very close to the diameter of C_{60}. The onions are almost always quasi-spherical in shape, as shown in Fig.3.4.

The detailed atomic structure of carbon onions has been the subject of much discussion. Some authors have assumed that the particles consist of nested fullerenes, as suggested by H.W. Kroto in the article which accompanied

Ugarte's paper. A plausible model for onion structure is one made up of concentric 'magic number' (or Goldberg Type I) fullerenes. These fullerenes have N carbon atoms, where $N = 60b^2$, so that the first five are C_{60}, C_{240}, C_{960} and C_{1500} (with all fullerenes having the I_h symmetry). In an onion constructed from these fullerenes, the spacing between successive shells would be ~0.34 nm, i.e. close to the interlayer spacing in graphite, and to the spacing observed experimentally for onions. A possible problem with this model is that most theoretical studies suggest that large fullerenes (C_{240} and larger) should be faceted, rather than spheroidal. Although this faceting is only evident in certain directions, as shown in Fig. 3.4, one would expect some of the onions in experimental images to appear quite strongly faceted, rather than spheroidal.

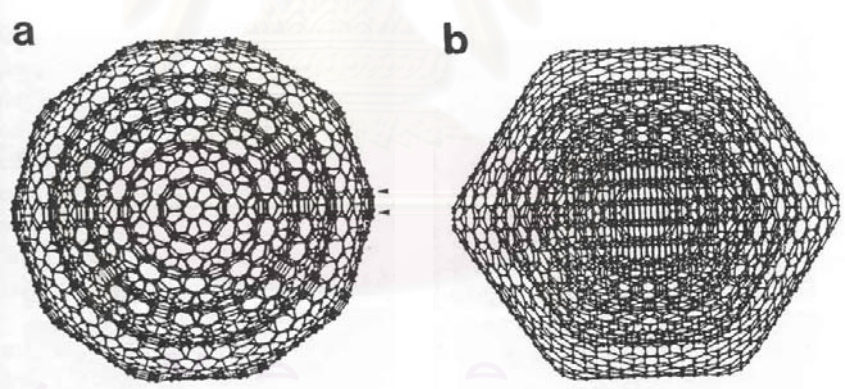

Figure 3.4 Two views of a five-shell carbon onion with the 'concentric fullerene' structure, along (a) C5 and (b) C2 symmetry axes [29]

However, work by a Japanese group led by Kunio Takayanagi has suggested that the onions become preferentially aligned with C_5 axis parallel to the beam, as a result of interaction with the magnetic field of the lenses, thus explaining their almost circular profiles. Detailed analysis of high resolution

images by Zwanger and Banhart has also provided support for the Goldberg-fullerene model.

Other workers have attempted to account for the sphericity of carbon onions by putting forward alternative structures. These have generally involved the introduction of heptagonal rings as well as pentagons into the structure of the carbon shells. The resulting structures are much more spherical than the corresponding fullerenes, as can be seen in Fig.3.5. This shows a shell containing 1500 carbon atom which contains 132 pentagons and 120 heptagons, taken from the work of Humberto and Mauricio Terrones. The sphericity of this structure suggests that it may represent a more realistic model for the outer shells of carbon onions than the 'perfect fullerene' model.

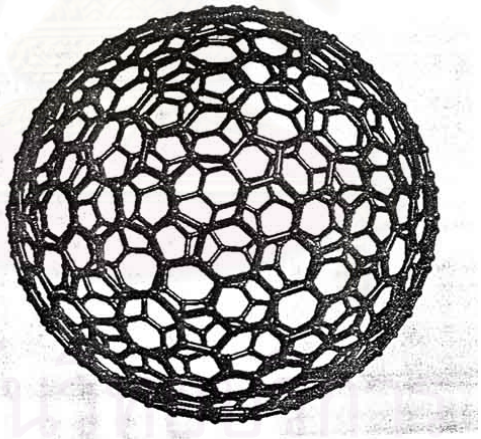

Figure 3.5 The Terrones model of carbon onion structure, incorporating pentagon-heptagon patches [29]

3.1.4 Carbon nanocapsules and multi-shelled carbon nanoparticles

It has been suggested that carbon-coated magnetic nanoparticles might have important applications in areas such as magnetic data storage, xerography

and magnetic resonance imaging. A typical example of carbon nanocapsule is shown in Fig. 3.6. It is a particle containing Xd encapsulated by graphene layers. The role of the carbon layer would be to isolate the particles magnetically from each other, thus avoiding the problems caused by interactions between closely spaced magnetic bits, and to provide oxidation resistance. In addition, the lubricating properties of the graphitic coatings might be helpful in magnetic recording and applications. The potential of important applications has motivated a significant amount of research on the encapsulation of magnetic materials in carbon nanoparticles.

Carbon nanocapsules which there are no metal as core particle can be called as multi-shelled nanoparticles. These particles consist several of graphene sheets in various shapes such as spherical, polyhedral, or short-tube.

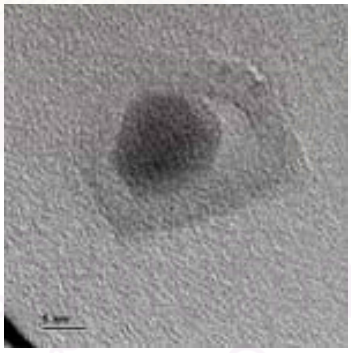

Figure 3.6 TEM image of Xd carbon nanocapsule [30]

3.1.5 Carbon nanohorns (CNHs) [31]

Another type of carbon nanoparticles is named nanohorns due to their irregular horn-like shape, and was discovered by Dr. Sumio Iijima's research group. Nanohorns have the same graphitic carbon atom structure as normal

carbon nanotubes. The structure of CNHs are shown in Figure 3.7. The main characteristic of the carbon nanohorns is that when many of the nanohorns group together an aggregate (a secondary particle) of about 100 nanometers is created. The advantage being, that when used as an electrode for a fuel cell, not only is the surface area extremely large, but also, it is easy for the gas and liquid to permeate to the inside. In addition, compared with normal nanotubes, because the nanohorns are easily prepared with high purity it is expected to become a low-cost raw material.

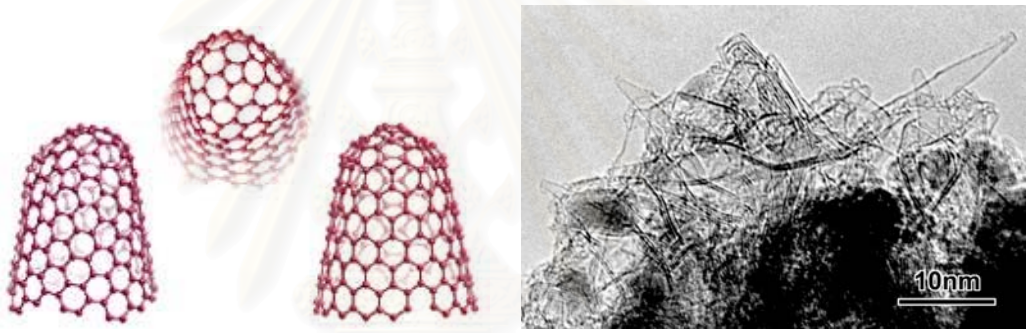

Figure 3.7 Carbon nanohorns (CNHs) model
and TEM image of CNHs [31,32]

The developed tiny fuel cell, classified as a polymer electrolyte fuel cell (PEFC), utilizes the carbon nanohorns as electrodes for catalyst support. It is observed that very fine platinum catalyst particles are dispersed on the surfaces of the carbon nanohorns. The size of the platinum particle is less than half of that supported on the ordinary activated carbon (acetylene black) by the same method. The size of the catalyst particle is one of the most important factors that determine the performance of the fuel cell, and it is considered that, the finer the size the better performance.

Although the reason a catalyst particle becomes fine is still not clear in the case of the carbon nanohorn, because of the unique shape of the aggregate it is thought that contact and grain growth of catalyst particles will be prevented. It is also expected that by further altering the form of the carbon nanohorn the dispersed state and the battery characteristic of the catalyst particle will improve. In addition, because a carbon nanohorn is produced by the laser ablation method, if a platinum catalyst is also simultaneously evaporated it is observed that a platinum particle will naturally adhere to the surface of a carbon nanohorn. If this method is used, the complicated catalyst supporting process through the conventional wet process can be omitted resulting in a large cost reduction.

3.2 Mechanism of carbon nanoparticles formation in an arc discharge submerged in water [2])

N. Sano *et al.* [2] have succeeded in fabrication carbon nanoparticles by using arc discharge submerged in distilled water. They have also proposed an informative explanation on the formation of those carbon nanoparticles. The mechanism proposed could be summarized as follow:

3.2.1 Gas bubble formation [2]

Two types of structures, carbon onions and elongated structures such as carbon nanotubes, were obtained in the water arc. Sano et. al. [2] proposed an initial model to explain the production mechanism of the two types of structures. Fig. 3.8 describes the model of the reaction zone. There is a plasma

zone between electrodes surrounded by a gas bubble due to vaporization of the surrounding liquid as the arc temperature is estimated to be around 4000 K (the sublimation temperature of carbon). In fact, this gas bubble can be regarded as a microwater-cooling reaction chamber that enables rapid quenching of the arc discharge. The main gas components are CO and H_2 produced by the reaction of C atomic vapor and H_2O at the gas-liquid interface as

$$C + H_2O \rightarrow CO + H_2 \qquad \ldots\ldots \qquad (Eq.3.1)$$

To produce CO at the gas-liquid interface, C atomic vapor must be present at this interface. It is therefore reasonable to expect that C atomic vapor exists wholly in the bubble surrounding the discharge.

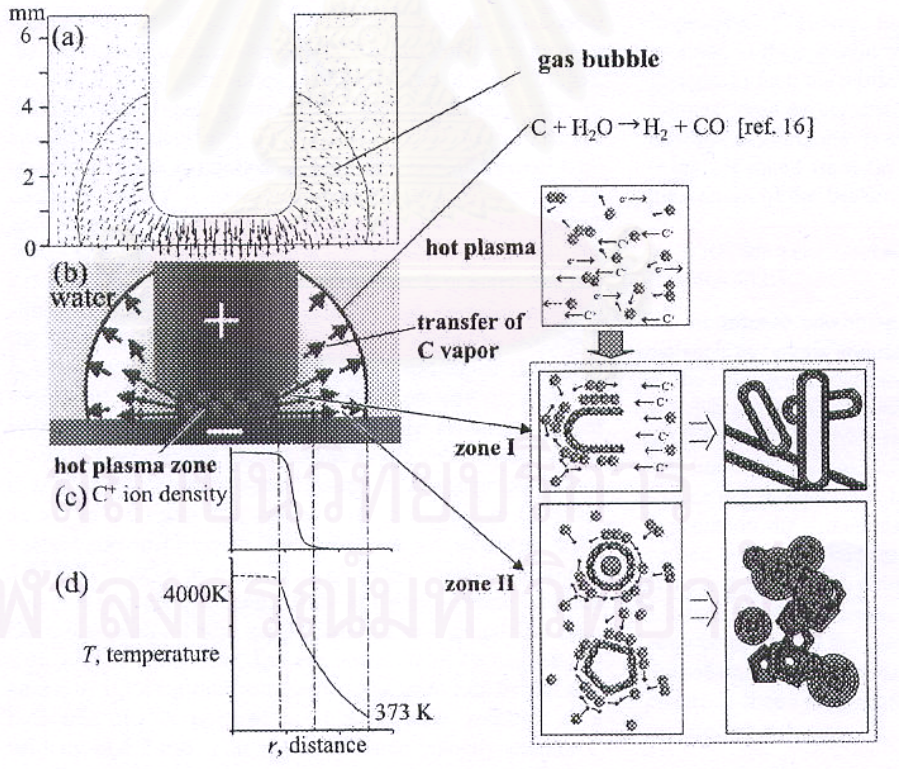

Figure 3.8 Formation mechanism of nanoparticles in a water arc. (Sano *et al*.,[2])

(a) Relative electric field strength, shown by arrows, between a rod anode and a flat cathode in a gas bubble surrounded by water

(b) Direction of thermal expansion from plasma to the water interface

(c) Quantitative ion density distribution.

(d) Temperature gradient obtained from Eq. (3.2) assuming qc, Q_R, and $dT/dt = 0$. The formation of elongated nanoparticles in zone (I) and onions in zone (II) is also shown schematically.

3.2.2 Nanoparticles formation [2]

The extremely sharp temperature gradient in this gas bubble from the hot plasma region to the gas-water interface is essential to cause rapid solidification of the vaporized carbon. The temperature at the hot plasma is estimated to be approximately 4000 K (The melting and boiling points of graphite are 3823 and 4203 K, respectively), while the temperature at the gas-water interface is the boiling point of water, 373 K.

To estimate the approximate temperature gradient, it can be simply assumed that the heat transfer occurs in a radial direction from the center of the plasma. Then the equation of heat balance can be expressed as:

$$-\frac{d}{dr}\left(4\pi r^2 q_k\right)-\frac{d}{dr}\left(4\pi r^2 q_c\right)+4\pi r^2 Q_R = 4\pi r^2 \rho C_p \frac{dT}{dt} \quad \text{..... (Eq.3.2)}$$

where r, q_r, q_c, Q_R, C_p, T, and t are the distance from the arc center, heat transfer rate by thermal conductivity, heat transfer rate by convection, reaction heat, density of gas, specific heat of gas, temperature, and time, respectively. To simplify the calculation, qc, Q_R, and dT/dt are assumed to be zero. If q_k is expressed by Fourier's law of thermal conductivity with a proportional constant k as $q_k = -k dT/dr$ with boundary conditions, T = 4000 K at r = 2 mm and T = 373

K at r = 5 mm, the average temperature gradient in the gas bubble is estimated to be 1209 K/mm. It is noted that this simple calculation is only to give a rough approximation of the temperature gradient.

In fact, qc, Q_R, and dT/dt should be significant in the real system and all parameters must be highly space and time dependent. Also, the expansion rate of C vapor from the hot plasma zone to cold region can be estimated by a simple approximation. If all the graphite consumed in the anode is assumed to be converted to C vapor, the volumetric C vapor expansion rate is calculated to be 5.30×10^{-5} m^3/s at 4000 K if ideal gas conditions with 1 atm pressure are assumed. If the hot plasma zone between electrodes with a 1 mm gap is assumed as a cylindrical zone with a 2 mm diameter, the expansion velocity can be obtained by dividing this volumetric expansion rate by the surface area of this assumed hot plasma zone, resulting in a velocity of 4.2 m/s. This high expansion velocity enables C vapor to transfer into the cold zone of the bubble readily. The cold zone can be categorized into two parts: (I) that where the quenching of C vapor occurs within the ion current adjacent to the hot plasma zone and (II) that without the ion current outside zone (I).

Although it had not been obtained the distribution of the ion current density in the system at present and it can be provided a map of simulated electric field in a configuration that is close to our electrode shapes in Fig.3.8a. This simulation does not include the effect of the C vapor expansion. In zone (I), elongated structures such as nanotubes are expected to be produced because of their epitaxial growth in the C ion current. On the other hand, in zone II,

three-dimensional (3D) isotropic growth of nanoparticles is preferable because of the absence of an axis of symmetry. In this case, onions may be produced.

3.2.3 Floatation of carbon nanoparticles [2]

Subsequent to the formation of onions, they cluster into larger van der Waals crystals. Sano *et al.* [2] find that these clusters readily float to the top of the water surface and these floating powder remains separates at the surface of the water even after vigorous dispersion through ultrasonication. In order to investigate the mechanism responsible for floatation of the onion powder by calculate the true density. It resulted in a mean density of particles of 1.64 g/cm^3. It is noteworthy that it is higher than water although it is lower than graphite 2.25 g/cm^3. The density is comparable to that of well known caged nanoparticles such as C_{60} and nanotubes whose densities are 1.72 and 1.2-2.0 g/cm^3 respectively. Hence, floatation of the particles cannot be ascribed to their weight but more likely to their hydrophobic surface. In fact, the particles can be dispersed well in organic solvents such as acetone, toluene and n-hexane. In their arc-in-water system, onions are naturally agglomerated and float, being separated from the other large products that settle to the bottom of the beaker.

CHAPTER IV

EXPERIMENTAL PROCEDURE

4.1 Experimental method

4.1.1 Arc discharge in organic compound

A schematic experimental apparatus for synthesize carbon nanoparticles (CNPs) is shown in Figure 4.1.

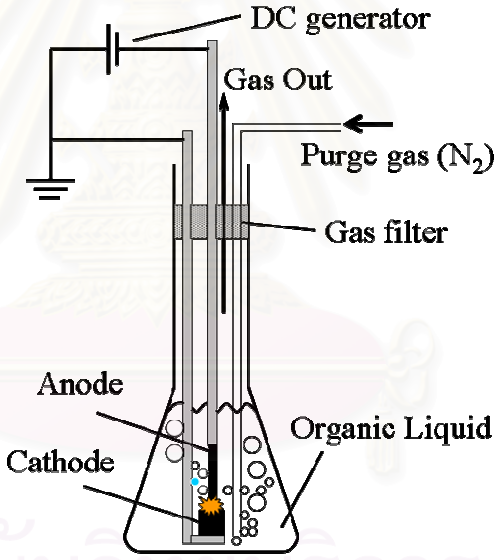

Figure 4.1 Experimental apparatus for arc discharge in organic liquid

A direct current (DC) welding power supply (IKURA ARC, IS-160D) was used to generate the arc plasma. Pure graphite electrode rods (99.999%, ToyoTanso) with diameters of 6 and 20 mm were used respectively as a movable anode and a cathode. The lengths of anode and cathode electrodes were 5 and 2 cm, respectively. These electrodes were aligned in vertical direction in

300 ml of liquid which was placed in a Pyrex glass flask with N_2 purging to prevent explosion during arcing. The N_2 gas with the flow rate of 1 l/min. was employed for 5 min. before starting the arc discharge and continuously purged until the arc discharge was stopped. The arc plasma was initiated by contacting two electrodes, and the gap between the electrodes were carefully controlled to be 1 mm to maintain stable discharge current of 50 A and voltage of 20-25 V for 3 min. The fluctuation of current and voltage were observed by ammeter and data recorder, respectively.

After the arc discharge was terminated, three types of products were found, (1) deposit at cathode end, (2) fine particles at the vessel bottom, and (3) deposit at anode end, and the vessel was leaved for 1 day to ensure that the dispersed particle was completely fell down at vessel bottom. These obtained products were collected and was washed by acetone and water, respectively. After that, these products were put in the oven for drying about 1 day, and were kept in sample bottles for analysis later.

4.1.2 Arc discharge in inorganic compound

The experimental set-up in this case is shown in Figure 4.2. The same DC welding machine in the previous case was employed. Both of the graphite cathode (20 mm diameter, 2 cm in length) and anode (6 mm diameter, 5 cm in length) were submerged to a depth of 3 cm in the 2.5 liters of salt solution. The solutions ($NiSO_4$, $CoSO_4$, $FeSO_4$, and Na_2CO_3) were prepared by weighting chemical powder and then dissolved these chemical by de-ionized water in Erlenmeyer flasks. The electrode holders were made from graphite which was

similar purity of electrodes to avoid the electrolysis phenomena during the experiment. The arc plasma was initiated by approaching the anode to the stationary cathode. The anode-cathode gap had elaborately been controlled to be 1 mm to maintain stable discharge current of 50 A and voltage of 20-25 V for arcing time of 10 min.

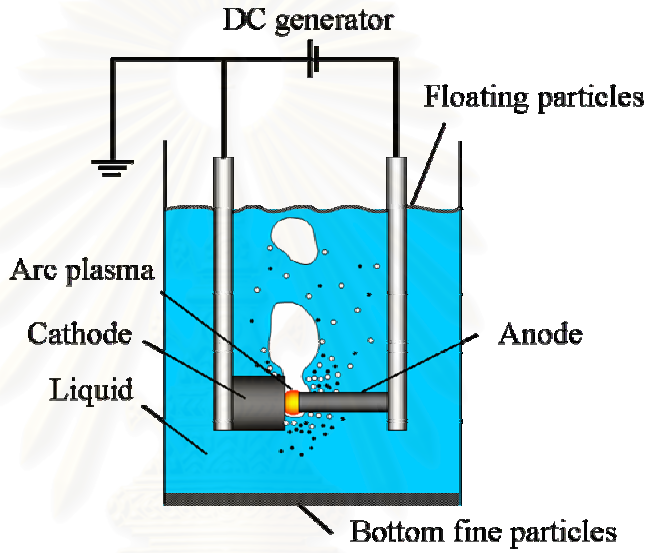

Figure 4.2 Experimental apparatus for arc discharge in inorganic liquid

Three types of products were observed after the arc discharge, cathode deposit, floating film particles, and sediment particles. The vessel was also left about 1 day for complete sediment of dispersed particle. After that, these obtained particles were collected and washed by de-ionized water for 5-6 times to remove some metallic compound which had remained in the samples. These products were dried in the oven for 1 day, and were kept in the sample bottles for analysis later.

4.1.3 Arc discharge in surfactant

The experimental set-up in this case was similar to the case of organic compound. De-ionized water, hexane (C_6H_{14}), and surfactant (mono-olein, $C_{17}H_{35}COOCH_2CH(OH)CH_2OH$) were used to prepare the liquid for arc discharge. The de-ionized water of 300 ml, hexane of 100 ml, and surfactant whose amount was varied as 0.0003, 0.003, 0.03, 0.3, and 3 g, were mixed in 2 liters beaker by using high-power ultrasonic disperser for 5 min. After leaving this liquid, it would be separated in two phases. This liquid was waited until that became equilibrium for 1 hour, and the water-rich colloid part was collected to be the liquid media for the experiment.

When the arc discharge was finished, two categorized of products had been observed, cathode deposit and sediment particles. To remove some emulsion which remained in the samples, acetone was used to rinse the sample. Next, the samples was dried and collected in the sample bottles for analysis later.

4.2 Preparation the samples for analysis

4.2.1 Transmission Electron Microscopy (TEM)

TEM specimens were elaborately prepared by gently grinding as-grown solid deposit by a mortar, subjecting to high power ultrasonic treatment (150 W) in toluene with sufficient time (1-2 min.) for ensuring its uniform dispersion and then transferred to a high-grade Cu grid coated with a porous carbon film. These specimens were loaded into sample chamber, waiting for 30 min. until it became steady state inside the chamber. After using TEM, the films were developed by using three chemical liquids in the dark room.

Figure 4.3 Transmission Electron Microscopy (TEM) (JEOL 2010)

4.2.2 Field Emission Scanning Electron Microscopy (FESEM)

FESEM specimens were prepared by grinding as-grown solid deposit by the mortar similar to TEM specimens, and then directly sprinkling the appropriate amounts onto a conductive carbon coated microscope grid. The specimens were loaded into sample chamber, and then immediately starting the observation with using image catcher scanner for taking the photos.

Figure 4.4 Field Emission Scanning Electron Microscopy (FESEM) (HITACHI, S-900)

4.2.3 Dynamic Light Scattering (DLS)

DLS was used to analyze the particle size distribution of the obtained products. It should be noted that DLS is based on the measurement of the dispersion of light scattering by particles motion in a static solvent such as

toluene, acetone or ethanol, the measured particle size should correspond to hydrodynamic diameter but not to the real diameters of the particles with complex structures. However, DLS results were expected to give at least the qualitative trend in particle sizes. Before the analysis, DLS specimens were also prepared by grinding as-grown particles by the mortar, and then subjecting to high power ultrasonic treatment (150 W) in toluene for 1 min. Next, the specimens were diluted by toluene until they became transparent, subjecting to ultrasonic disperser again for 1 min. and then loading to the sample cell for analysis. The Dynamic Light Scattering (DLS) machine is shown in Figure 4.5.

Figure 4.5 Dynamic Light Scattering (DLS)
(MALVERN ZETASIZER300HSA)

4.2.4 Raman Spectroscopy

As-grown substrate of solid deposit was filled into the hole of specimen holder and then was bombarded by an Ar ion laser (514 nm) at the room temperature. In the cases of carbon nanoparticles (CNPs), two peaks can be

found in the wavenumber between 1200 and 1800 cm^{-1}. One is a strong peak at 1590 cm^{-1} (Graphite band, G band) arises from an in-plane oscillation of carbon atoms in the sp^2 graphene sheet. Another is a weak peak at 1340 cm^{-1} (Disordered band, D band) reflects the degree of defects or dangling bonds contained in the sp^2 arrangement of graphene sheet. The Raman spectroscopy machine is shown in Figure 4.6.

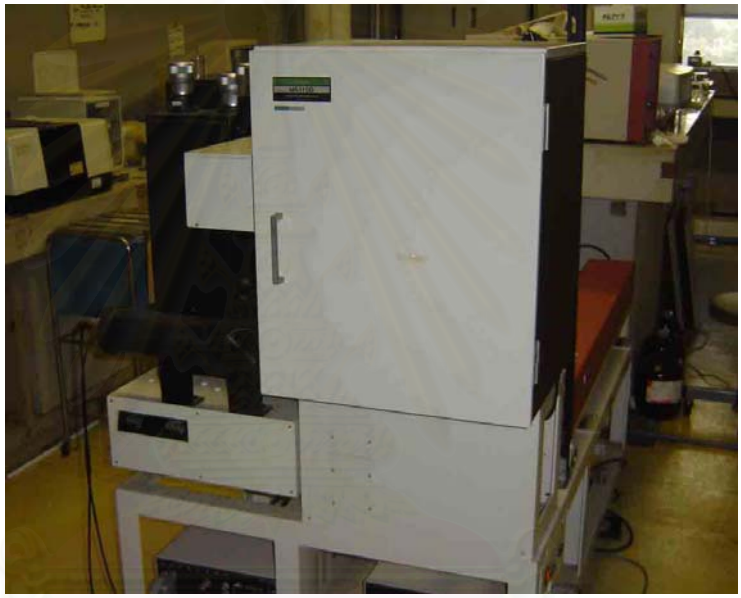

Figure 4.6 Raman Spectroscopy (JASCO, NR1100)

4.2.5 Ultraviolet-visible light (UV-vis) absorption spectrometer

The UV-vis spectrometer is shown in Figure 4.7. UV-vis was employed to analyze the absorption of sample compared with that of standard liquid. Before the analysis, two sample cells were prepared. One was for loading the liquid sample; another was for loading the standard liquid. The UV-vis spectra give the data about the difference of compounds which contained in the liquid samples as the function of the absorbance and wavelength.

Figure 4.7 UV-vis absorption spectrometer (Shimadzu, UV-1600PC)

CHAPTER V

RESULTS AND DISCUSSION

5.1 Influence of organic compounds

5.1.1 Influence of molar ratio of H_2O-C_2H_5OH and H_2O-CH_3OH mixtures

5.1.1.1 Phenomena observed during the arc discharge

Since organic compounds contain some certain amount of carbon atoms in their molecules, it is reasonable to expect that using a mixture of organic compound and water to accommodate arcing might help provide additional carbon atoms to engage in carbon nanoparticles forming reaction.

The phenomena observed during the arc discharge in H_2O-C_2H_5OH mixture are shown in Table 5.1. This reveals that with an increase in C_2H_5OH concentration, the arc plasma tends to be more stable and then provides some hard deposits at the end of anode, which could be observed as shiny (gray) deposition at the anode tip.

From Table 5.1, ‘very stable’ arc plasma is determined from observation that the brightness of plasma is continuously stable and the applied voltage is almost stably controlled at 1.5 V.

Table 5.1 Arc stability and the residual liquid color after arc discharge in C_2H_5OH-H_2O mixtures with varying concentration

Concentration	**C_2H_5OH**				
vol %	**0**	**25.0**	**50.0**	**75.0**	**100**
wt %	**0**	**20.8**	**44.1**	**70.3**	**100**
mol %	**0**	**9.3**	**23.6**	**48.1**	**100**
1. Stability of arc plasma	O	O	O	**OO**	**OO**
2. Color at the anode tip	B	B	**S**	**S**	**S**
3. Residual liquid color	X	light yellow	yellow	light brown	brown
4. UV-VIS graph area (nm)	0	0.2	0.3	1.6	36.9

Note: O = stable, OO = very stable, X = colorless, B = black, S = shiny

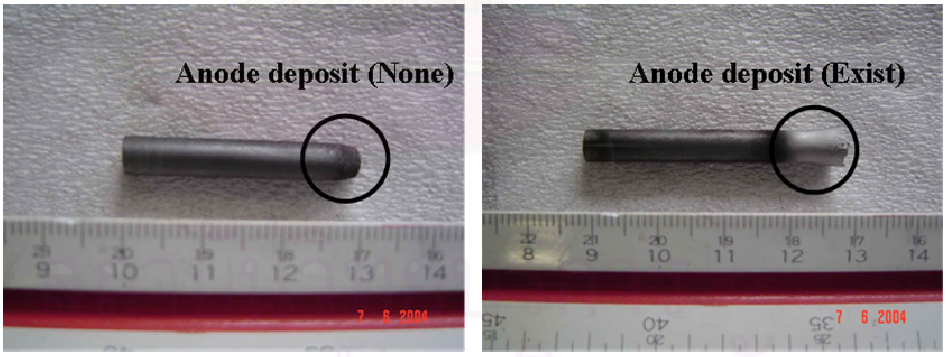

Figure 5.1 Anode electrode after arcing in de-ionized water (left) and pure C_2H_5OH (right)

Figure 5.1 shows the anode deposit which could not be found by arc in water but in the pure C_2H_5OH, the deposition exhibits grayish or shiny apparance.

Moreover, some of organic compounds as byproducts were also generated in residual liquid during the arc discharge as could be observed from the liquid color (Table 5.1). It could be suggested that UV-VIS absorption analysis should be conducted to investigate the absorbance of residual liquid. It can be seen from Table 5.1 that the condition of 25, 50, 75, and 100% vol, the color of the residual liquid changed into light yellow, yellow, light brown to brown, respectively. Based on this result, it could be implied that the amounts of these by-products might increase with the increasing concentration of C_2H_5OH. The integrated graph areas of UV-VIS absorption spectra were also shown in Table 5.1. It reveals that the integrated graph area increases with the increasing concentration of C_2H_5OH, confirming that concentration of by-products became higher as the concentration of C_2H_5OH was increased.

In the case of CH_3OH-H_2O mixtures, it can be seen from Table 5.2 that the increasing concentration of CH_3OH could result in more stable arc plasma similar to that of C_2H_5OH-H_2O mixture. While the color of hard deposit at the anode tip is black, the surface of hard deposit at the anode tip was shiny only when pure CH_3OH was employed.

The obtained residual liquid became visually colorless similar to that of ‘arc in water’ system. However, from the UV-VIS analysis, the absorbance of the residual liquid before and after the arc discharge are different, leading to a conclusion that some colorless organic compounds were produced as by-products in the residual liquid. Moreover, the concentration of the by-product organic compounds increases with the increasing concentration of CH_3OH similar to that of C_2H_5OH system. Through there are no quantitative analysis

conducted in this work, these residual liquids might be expected to contain polyynes which were detected by F. Cataldo [33]. It is reported that H-terminated polyynes could be obtained by using submerged arc in organic solvents such as methanol and hexane in the conditions similar to this work.

Table 5.2 Arc stability and the residual liquid color after arc discharge in CH_3OH-H_2O mixtures with varying concentration

Concentration	**CH_3OH**				
vol%	**0**	**25.0**	**50.0**	**75.0**	**100**
wt %	**0**	**20.9**	**44.2**	**70.4**	**100**
mol %	**0**	**12.9**	**30.8**	**57.2**	**100**
1. Stability of arc plasma	O	O	O	O	**OO**
2. Color at the anode tip	B	B	B	B	**S**
3. Residual liquid color	X	X	X	X	X
4. UV-VIS graph area (nm)	0	0.6	1.5	11.6	41.3

Note: O = stable, OO = very stable, X = colorless, B = black, S = silver

5.1.1.2 Microscopic analyses of the obtained products

After the arc discharge, three types of products, cathode deposit, sedimentary particles and anode deposit (shiny color) could be observed. Generally, no anode deposit could be observed from arc discharge in water. In this work, there are no floating particles obtained from arc discharge in C_2H_5OH-H_2O and CH_3OH-H_2O mixtures.

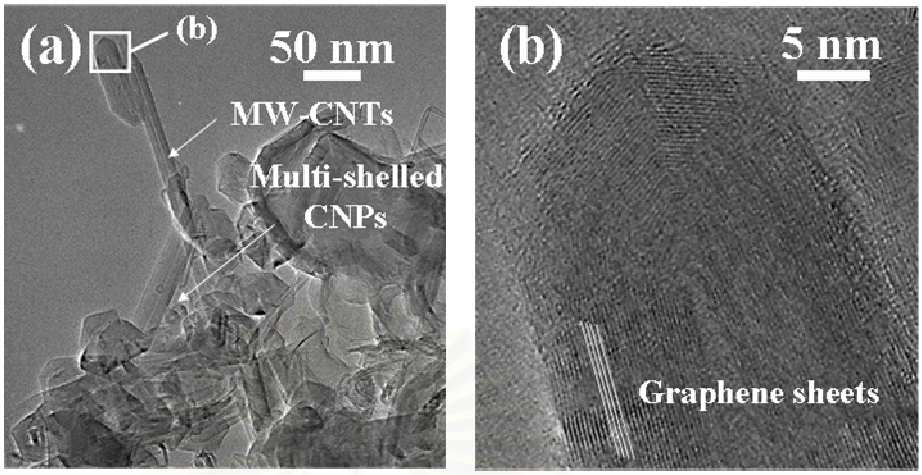

Figure 5.2 TEM images from arc in pure C_2H_5OH, (a) cathode deposit which mainly consists of MW-CNTs and multi-shelled CNPs, and (b) high magnification image of obtained MW-CNTs

Microscopic analyses shown in Figure 5.2 reveal that cathode deposit obtained from arc in C_2H_5OH-H_2O contains the mixed CNPs which are MW-CNTs with nominal diameter of 10-30 nm and length of 70-400 nm, and multi-shelled carbon nanoparticles with diameters of 20-50 nm. These mixed products were seen everywhere by scanning observations, indicating that the purity of CNPs is very high. It should be noted that the CNPs concentration of 65-70% could be estimated experimentally.

The main structures of the products collected from vessel bottom were crystalline and amorphous carbon nanoclusters as shown in Figure 5.3. However, an extremely low concentration of CNPs was observed in pure C_2H_5OH system, whereas the concentration of CNPs in bottom products increases to 40-50% in systems of C_2H_5OH-H_2O mixture. With ‘arc in water’ condition (concentration of C_2H_5OH is zero), amount of CNPs in the bottom

products goes up to about 50%. This might be implied that because the quenching rate in C_2H_5OH is higher than that in water. The electrodes deposit could become more enhanced, resulting in lower amount of sediment product. In the anode deposit, all were graphite and disordered carbons, and CNPs were not found.

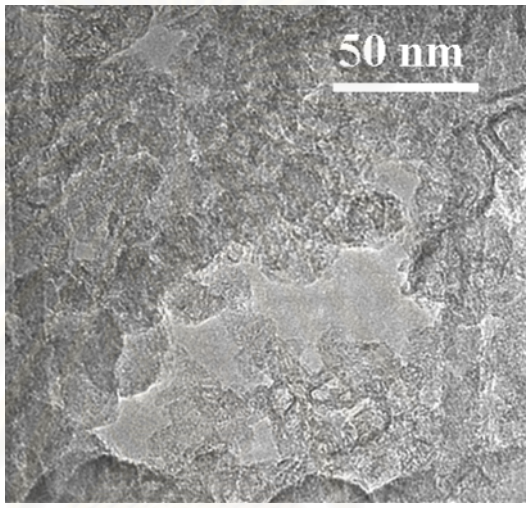

Figure 5.3 TEM images from arc in pure C_2H_5OH, bottom particles which mainly consist of graphite and amorphous structures

For systems of CH_3OH-H_2O mixtures, typical FESEM images of the synthesized products are shown in Figure 5.4. As the cathode deposit, CNPs which contain MW-CNTs and multi-walled carbon nanoparticles can be obtained, similarly to the products of 'arc in C_2H_5OH' system. Interestingly, CNPs were found not only in the cathode deposit but also in the sediment at the reactor bottom in all conditions. It is also found that the concentration of CNPs in the cathode deposit is higher than that in the bottom products. It should be reminded that CNPs were not found in the bottom products in the C_2H_5OH systems. Meanwhile, the anode deposit obtained from CH_3OH-H_2O

mixtures mainly consisted of graphite and amorphous carbon similar to that of C_2H_5OH-H_2O systems.

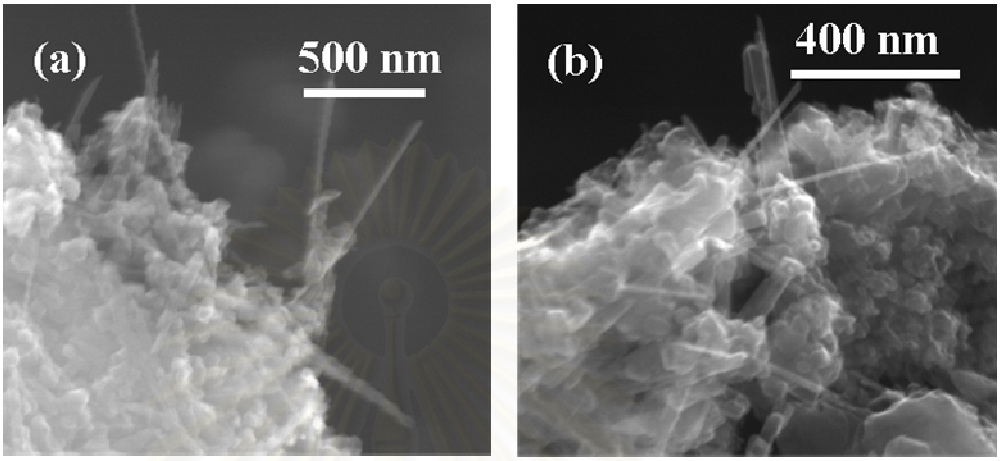

Figure 5.4 FESEM images from arc in pure CH_3OH,

(a) cathode deposit, and (b) sediment particles

5.1.1.3 Production rate and yield

The production rate and the yield of the products obtained from arc in C_2H_5OH-H_2O mixtures are shown in Figure 5.5. The production rate is analyzed regarding to each category of deposite.

The formation rate of the cathode deposit slightly decreases as the concentration of C_2H_5OH is increased within a low concentration range (< 10 mol %). Over this concentration, it oppositely increases with the increasing C_2H_5OH concentration up to 3.5 g/h, which is approximately 4.5 times higher than that of arc in water.

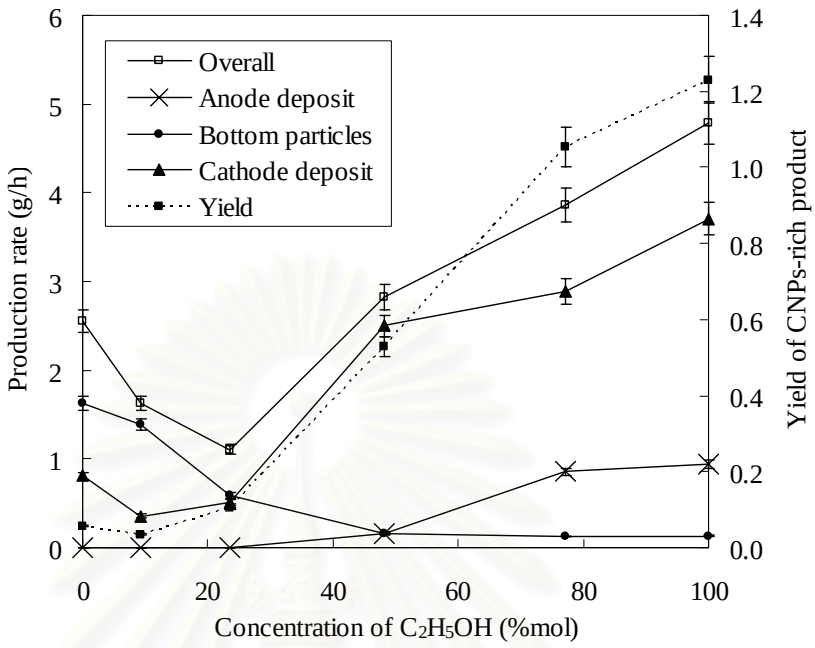

Figure 5.5 Influence of the concentration of C_2H_5OH on the production rate and yield of obtained products

The increase in the production rate in the C_2H_5OH system can be explained as a result of the increasing carbon vapor content in gas bubbles emerging by the arc. When pure C_2H_5OH is used, 4.17×10^{19} atoms/m^3 of carbon should theoretically exist in the bubbles regarding to its vapor pressure. This value was theoretically estimated from PV = nRT, when P = 1 atm, R = 82.057 atm.m^3/gmole.K, T = 78.4 ^oC (boiling pt. of C_2H_5OH) and 1 gmole = 6.02×10^{23} atoms. Furthermore, the higher latent heat of vaporization of C_2H_5OH compared with water might also lead to an additional increase in the quenching rate. This implication would be proofed by measuring the heat absorbed in pure C_2H_5OH compared with that in H_2O. It is known that the heat released from arc plasma can be estimated from power and efficiency of the

generator. Accordingly, it is found that the efficiency of heat absorption in C_2H_5OH and H_2O cases are 77.6% and 60%, respectively. Therefore, when the concentration of C_2H_5OH is increased, the higher rate of heat removal could be expected, resulting in the lower formation rate of bottom products and more anode deposit.

The yield of CNPs-rich cathode deposit was determined from the ratio of the weight of cathode deposit to that of consumed anode. When this value is higher than unity, it suggests that carbon source for CNPs formation is not only the graphite electrode but also the liquid. It can be clearly seen in Figure 5.5 that in the case of pure C_2H_5OH, the production yield is 123%. Therefore, this result implies that C_2H_5OH could play a role as the carbon source for producing CNPs. In contrast, for 'arc in water' system, carbon atoms are supplied only from the graphite electrodes, resulting in a low production yield which is approximately 0.1. It is noteworthy that the yield of CNPs-rich cathode deposit from pure C_2H_5OH is about 12 times higher than that of the conventional 'arc in water'. This result shows that the carbon source for 'arc in C_2H_5OH' is mainly from C_2H_5OH.

In the case of CH_3OH-H_2O mixtures, the production rate and yield of the products are shown in Figure 5.6. This figure shows that the 'arc in water' results in the highest overall production rate of 2.6 g/h. The formation rate of cathode deposit slightly decreases as the concentration of CH_3OH is increased until the concentration of CH_3OH about 10-15 %mol. Over this concentration, the production yield significantly increases with the increasing concentration. Furthermore, when the concentration of CH_3OH increases, the quantity of

bottom products decreases while the anode deposit increases. The overall production rate decreases as the concentration of CH_3OH becomes higher. The yield of CNP-rich cathode deposit increases with the increasing concentration of CH_3OH. This is similarly explainable as the increasing concentration of CH_3OH leads to an increase in the carbon atoms in the emerging gas bubbles. As previously demonstrated by the ideal gas law, there are $2.17x10^{19}$ carbon atoms/ cm^3 in the emerging gas bubbles for pure CH_3OH system.

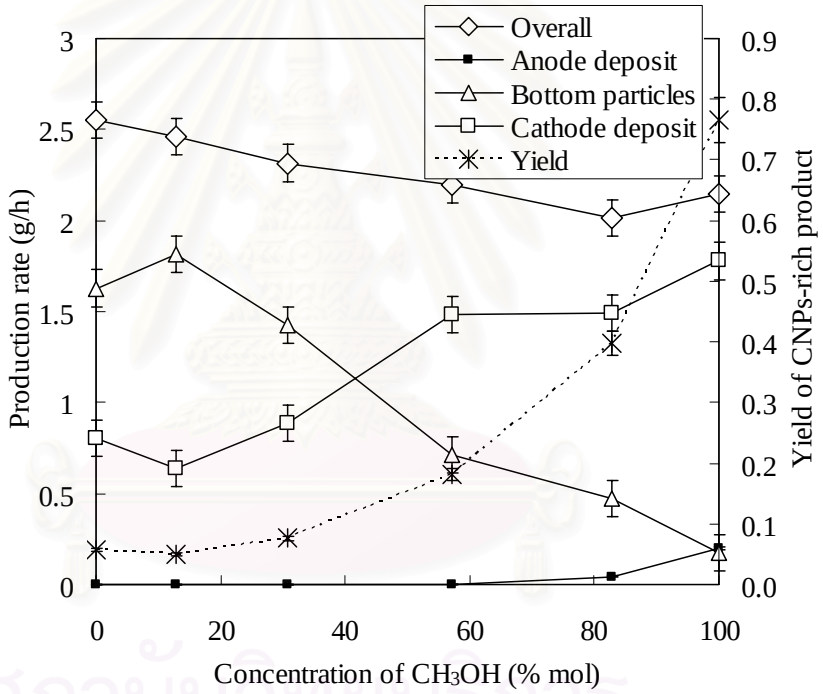

Figure 5.6 Influence of the concentration of CH_3OH on the production rate and yield of obtained products

5.1.1.4 Particle size distribution

Typical average particle sizes of the CNPs-rich deposits evaluated by DLS are shown in Figure 5.7. It is known that particle size distribution of the obtained product is typically log-normal.

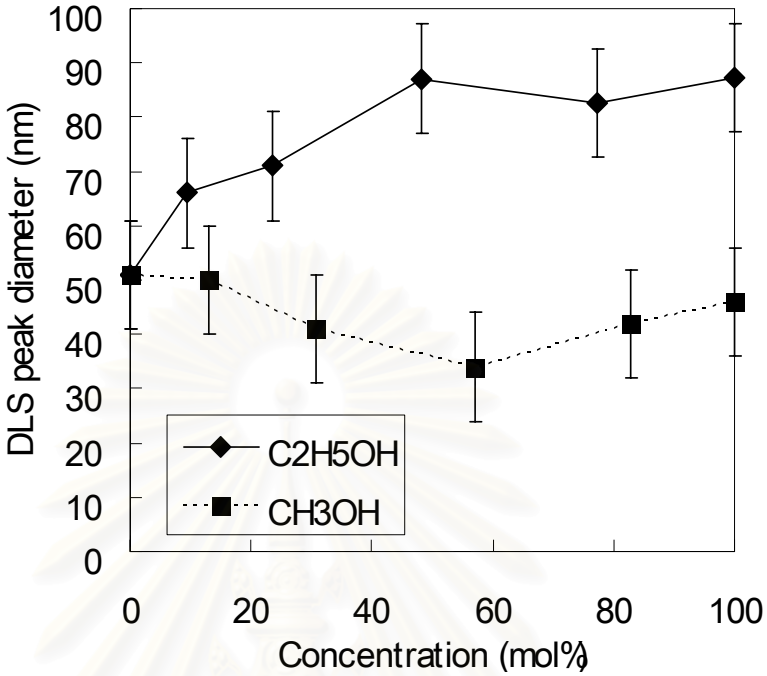

Figure 5.7 Influence of the concentration of alcohols on the particle size distribution of CNP-rich products

For the CH_3OH systems, it can be seen that the mean hydrodynamic diameter is between 25-60 nm. For the C_2H_5OH systems, the mean hydrodynamic diameter of CNPs lies in a range of 40-100 nm. Moreover, the mean diameter of the products obtained from C_2H_5OH system slightly increases with the increasing concentration. Based on this result, it could be implied that the selectivity of elongated-structures in C_2H_5OH is higher than in H_2O, because the concentration of carbon atoms in C_2H_5OH system is much higher than in H_2O, leading to the enhanced growth of elongated particles which need more carbon-supply. In addition, the mean diameter of CNPs from C_2H_5OH is higher than that from CH_3OH. This is because the quantity of carbon atoms in C_2H_5OH system is higher than that in CH_3OH system with the

same concentration, resulting in the higher growth of elongated structures in C_2H_5OH system.

5.1.1.5 Raman spectroscopic analysis

The ratio of the intensity of graphitic band (G-band, 1580 cm^{-1}) to that of disorder band (D-band, 1353 cm^{-1}) in the Raman spectra of CNPs-containing deposits are shown in Figure 5.8.

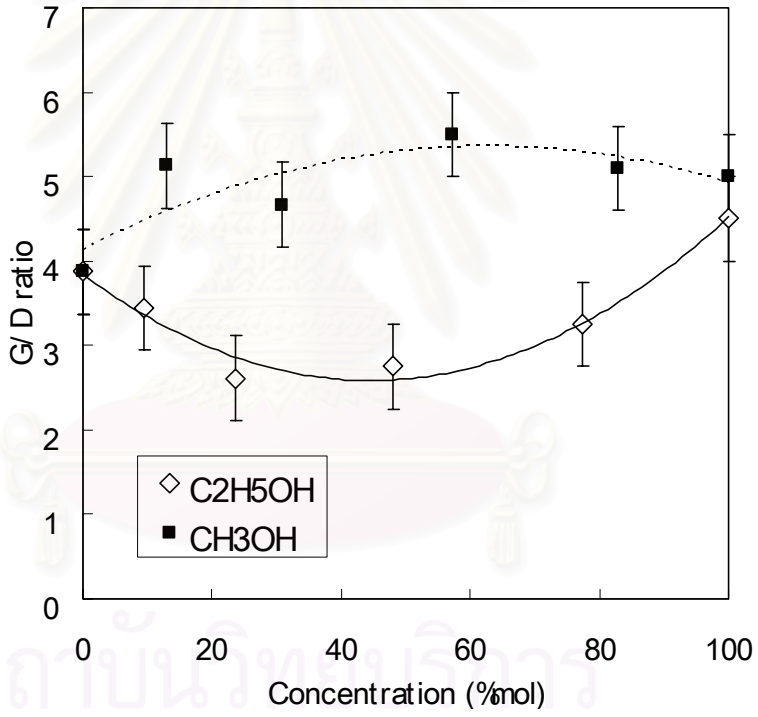

Figure 5.8 Influence of the concentration of alcohols on the G/D ratio of CNP-rich products

With an increase in the concentration of C_2H_5OH, the G/D ratio of the obtained CNPs deviates within a range of 2.7 to 4.5. The G/D ratio becomes highest when pure C_2H_5OH is used and becomes lowest when 30 mol% of

C_2H_5OH is employed. This might be attributed that in the range of 0-30 mol%, oxidative species induced from H_2O could react with carbon atoms to terminate the CNPs growth, resulting in their structural defects. Above the 30 mol% concentration, higher concentration of carbon atoms from C_2H_5OH may support continuous growth of CNPs, leading to the increase in G/D ratio. On the other hand, for the cases of CH_3OH, the G/D ratio is not significantly sensitive to the change of CH_3OH concentration through the ratio is slightly higher than that of C_2H_5OH.

5.1.1.6 Evaporation rate of the liquid

Even though more carbon atoms could be expected from the alcohols as the additional carbon source, it is inevitable that higher liquid lost is encountered due to its higher vapor pressure.

The evaporation rate of liquid was obtained by measuring the decrease of the liquid volume with respect to the arcing time. In the case of pure C_2H_5OH, the weight of consumed anode and the weight of overall solids products were 0.15 g and 0.24 g, respectively. Therefore, it should be expected that C_2H_5OH supplied 0.09 g of carbon to form the obtained products. The decrease in C_2H_5OH volume during the experiment was 110 ml which corresponds to 86.5 g of C_2H_5OH. Thus, most of C_2H_5OH was lost by evaporation. Similarly, the consumption CH_3OH liquid was also caused mainly by vaporization. It could be seen from Figure 5.9 that the evaporation rates become higher with the increasing concentration of alcohol, and the

evaporation rate of C_2H_5OH is lower than that of CH_3OH. This is an expected result due to the effect of vapor pressure difference as discussed above.

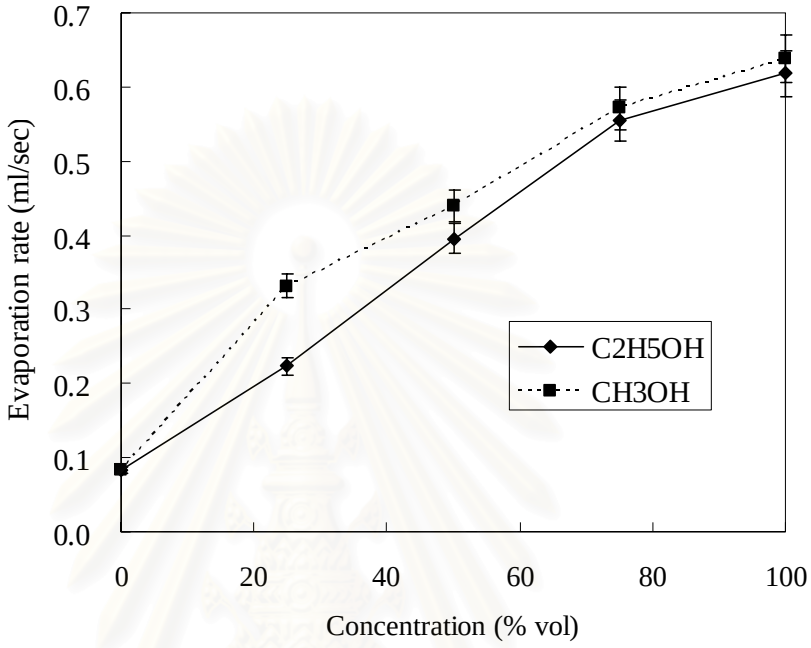

Figure 5.9 Influence of the concentration of alcohols on the evaporation rate of liquid during the arc discharge

5.1.2 Influence of number of C atoms in n-alcohol ($C_mH_{2m+1}OH$, m=1-8)

5.1.2.1 Phenomena observed during the arc discharge

The n-alcohols of various molecular weight ($C_mH_{2m+1}OH$, m=1-8) were employed as liquid media to accommodate the arc. In this work, pure alcohols were employed because of the difference in their solubility especially for high molecular weight of alcohol. The phenomena observed during the arc discharge in each alcohol are shown in Table 5.3. It can be seen that arc plasma in all cases was very stable. This result could be summarized that the increase in carbon atoms in the alcohol could help accommodate higher stable arc plasma.

Table 5.3 Arc stability and the residual liquid color after arc discharge in alcohols with varying carbon numbers

Substances	**Alcohol**							
Number of carbon atoms In molecule (m)	**1**	**2**	**3**	**4**	**5**	**6**	**7**	**8**
1. Arc plasma	OO	OO	OO	OO	OO	OO	OO	OO
2. Residual liquid color	X	light yellow	yellow	dark yellow	light orange	orange	black	orange

Note: OO = very stable X = colorless

Additionally, various organic byproducts were also generated in the residual liquid exhibiting different colors as shown in Table 5.3 and Figure 5.10. Typical UV-VIS absorption spectra of the residual liquids are shown in Figure 5.11. It could be seen that the components and amount of byproducts are different depending on number of carbon in each alcohol.

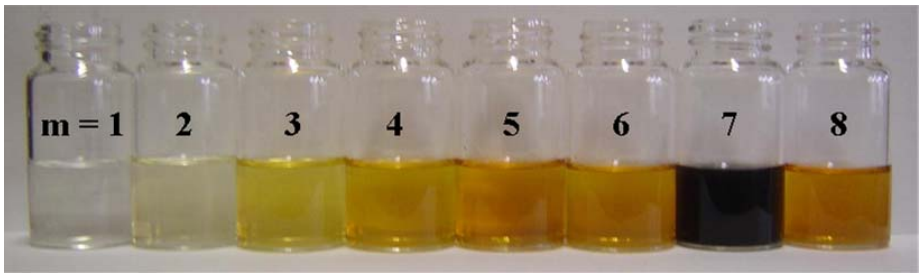

Figure 5.10 Color of residual liquid by arc in alcohol ($C_mH_{2m+1}OH$)

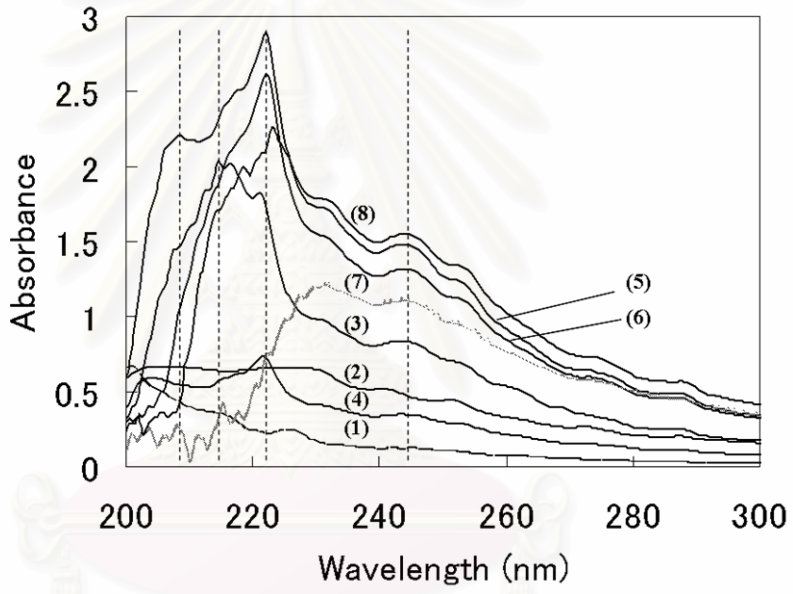

Figure 5.11 UV-VIS absorbance spectra of residual liquid in alcohol cases

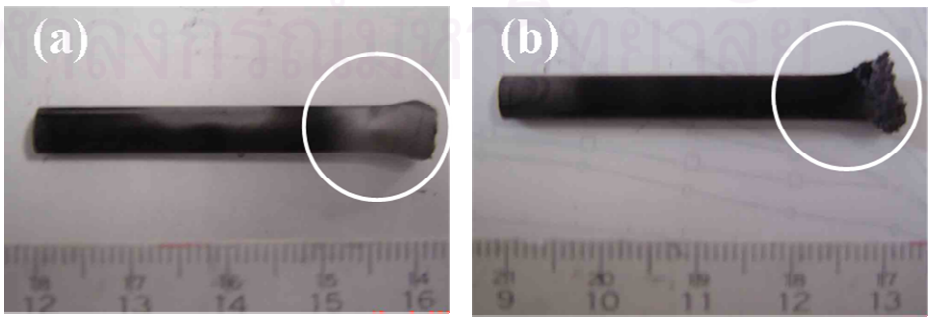

Figure 5.12 Anode electrode after the arc discharge in

(a) Propanol (m=3) 100%, (b) Hexanol (m=6) 100%

Furthermore, different anode deposit could be obtained from arc in different alcohols as shown in Figure 5.12. With a higher molecule weight alcohol more amount of anode deposite could be produced due to the higher continuously supplied carbon atoms from alcohols.

5.1.2.2 Microscopic analyses of the obtained products

Microscopic analyses of products synthesized by arc in alcohols are conducted by FESEM and TEM shown in Fig. 5.13.

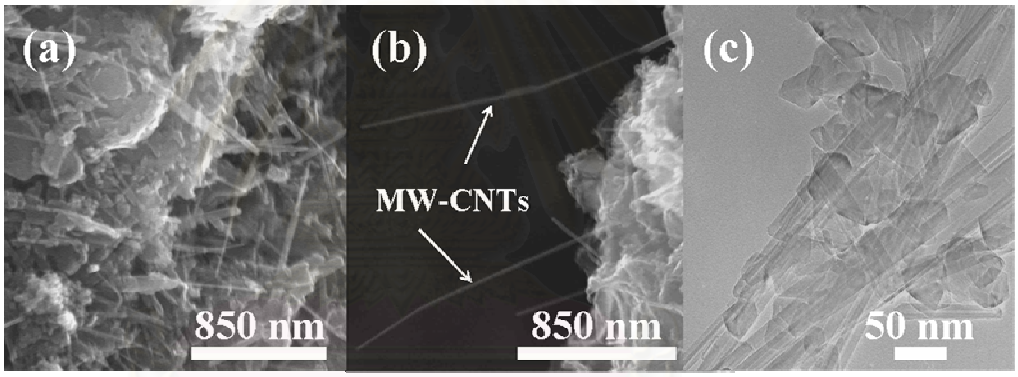

Figure 5.13 Microscopic analyses from cathode deposit product, (a) FESEM image from Pentanol (m=5) 100%, (b) FESEM image from Octanol (m=8) 100%, and (c) TEM image from Heptanol (m=7) 100%

Figure 5.13 reveals that cathode deposits contain high concentration of CNPs which are also MW-CNTs and multi-shelled CNPs. It should be noted that the obtained MW-CNTs exhibit diameter of 10-20 nm and length of 400 nm to more than 1 μm while the multi-shelled CNPs have diameter of about 20-70 nm. Additionally, other carbon structures including graphite and

amorphous carbons are also found. Concentration of the obtained CNPs is more than 70% based on scanning observation. The main products in the bottom particles are graphite and amorphous carbon. It can be observed that the concentrations of CNPs in the sediment are less than 5%. In the anode deposit, major products are graphite and disordered carbon, and CNPs could not be observed.

5.1.2.3 Production rate and yield

The production rate of products shown in Figure 5.14a suggests that when the number of carbon atoms (m) becomes higher, the overall production rate and the production rate of the cathode deposit are increased until m = 6. Over this point, the production rate becomes depressed. The bottom particles slightly increase with the increasing numbers of carbon. The relationship between the yield of CNPs-rich deposit (cathode deposit) and the number of carbon in the employed alcohol is also shown in Figure 5.14b. The yield become higher up to the highest value of 10 to m = 7 as the carbon atoms is increased. It should be reminded that the obtained yield from arc in water is about 0.1. Based on this result, highest yield obtained from arc in heptanol is about 100 times as that in the conventional ‘arc in water’ condition. Therefore, it can be concluded that the main carbon source of ‘arc in alcohol’ should be from liquid alcohol.

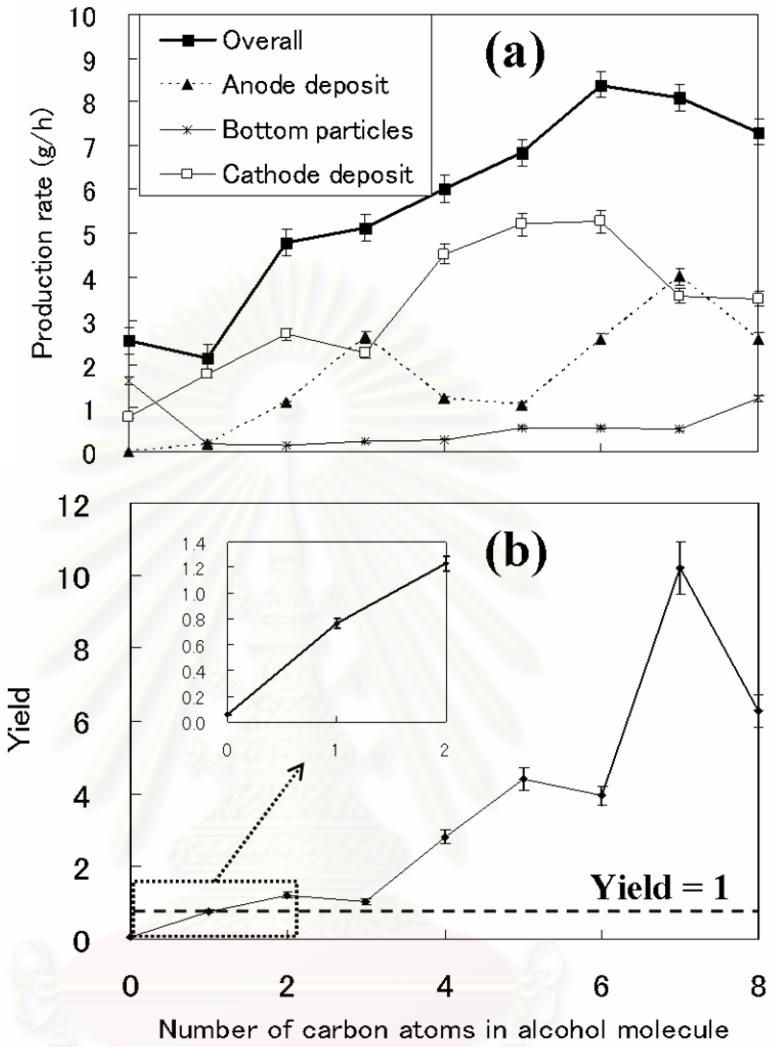

Figure 5.14 Influence of the number of carbon atoms in alcohol molecule on

(a) production rate of obtained products,

(b) yield of CNPs-rich product

5.1.2.4 Particle size distribution

Average particle size obtained from particle size analysis by DLS as shown in Figure 5.15 reveals that, in all cases of the ‘arc in alcohol’ the obtained CNPs exhibit different size ranging from 40 to110 nm. Interestingly, all of alcohols except methanol give rise to the CNPs with mean diameter

larger than that of arc in water. This can be implied that the selectivity of MW-CNTs to other CNPs obtained from arc in alcohol is higher than that from ‘arc in water’. This is consistent with microscopic analysis because the concentration of carbon in liquid is higher than that in water, resulting in the higher growth of elongated-shape CNPs.

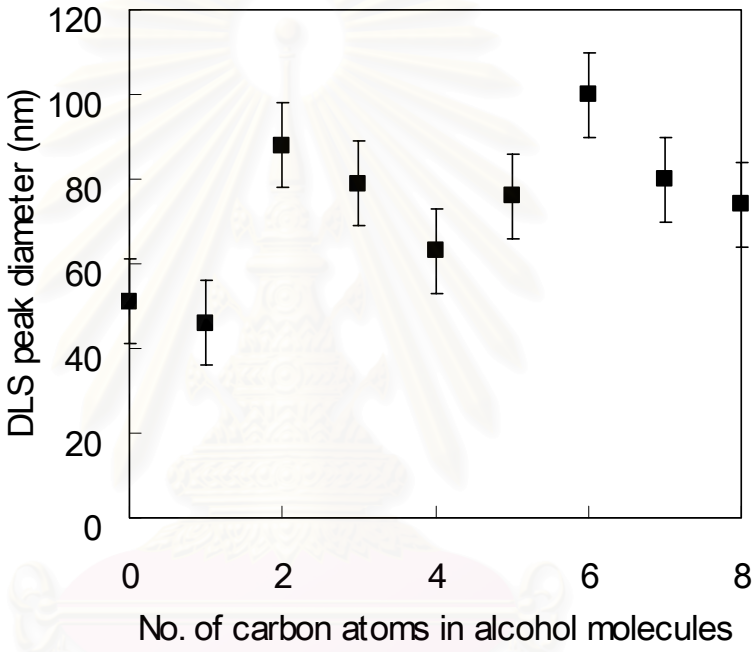

Figure 5.15 Influence of the number of carbon atoms in alcohol molecule on DLS peak diameter of CNPs-rich product

5.1.2.5 Raman spectroscopic analysis

The G/D ratios of the CNPs obtained from arc in alcohols are shown in Figure 5.16. This shows that when carbon number increases, the G/D ratio become lower until m = 5. Above this point, it becomes inversely higher. This result could be implied that in obtained product consist of CNPs and other carbon structures including crystalline, amorphous carbon cluster. The

tendency of graph became Figure 5.16 because of the difference in quantity of these non-CNPs particles.

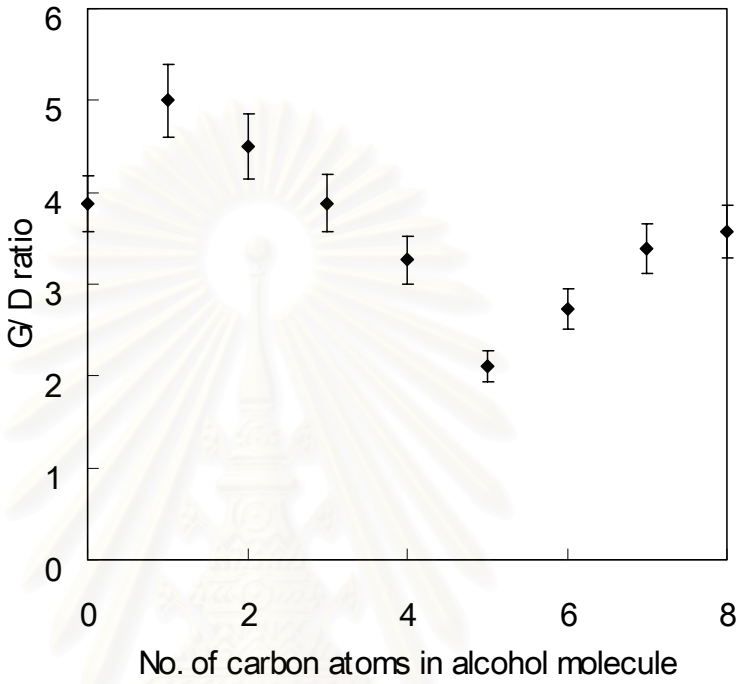

Figure 5.16 Influence of the number of carbon atoms in alcohol molecule on the G/D ratio of obtained product

5.1.2.6 Evaporation rate of the liquid media

The consumed anode and overall product weights in n-heptanol case (m=7) were 0.01 and 0.4 g, respectively. Then, the synthesized particles needed carbon source n-heptanol as carbon source about 0.39 g. However, the consumed liquid during the arc discharge was about 16.1 g of n-heptanol. From the experimental results of alcohol-H_2O mixtures discussed previously, it could be clearly seen that the alcohols were vaporized during the arc. Then, comparison of evaporation rate of each pure alcohol is shown in Figure 5.17.

It can be seen that the evaporation rate of alcohol becomes lower with the increasing carbon number in the alcohol molecule because in alcohol of larger molecules, stronger Van der Waals interaction can be expected and reflux as higher latent heat of vaporization.

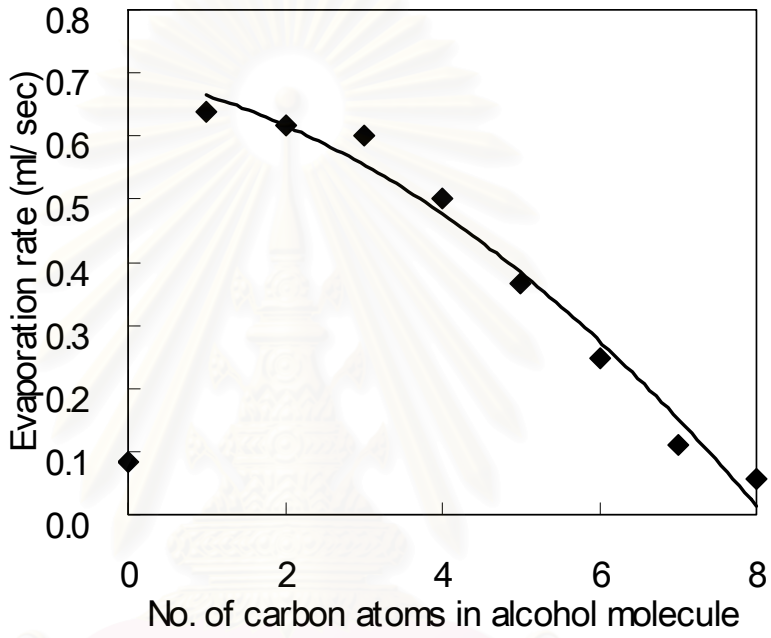

Figure 5.17 Influence of the number of carbon atoms in alcohol molecule on the evaporation rate of liquid during the arc discharge

5.1.3 Influence of number of C atoms in n-alkanes (C_mH_{2m+2}, m=6-7)

5.1.3.1 Phenomena observed during the arc discharge

In this work, n-alkanes were utilized as liquid for arcing. It is expected that n-alkanes would give results better than that of alcohols because there are no oxygen existing in alkane molecules, resulting in no side reaction from oxygen is occurred. The n-alkanes which have relatively high molecular weights (C_mH_{2m+2}, m=6,7) were employed since C_mH_{2m+2} (m=1-4) are gas phase at ambient condition as well as the vapor pressure of C_5H_{12} is so high that it is difficult to conduct stable experiment. After the arc discharge, the phenomena observed from arc in alkanes are shown in Table 5.4. It can be seen that arc plasma in all cases was very stable.

Table 5.4 Arc stability and the residual liquid color after arc discharge in alkanes with varying carbon numbers

Substances	**Alkane**	
Number of carbon atoms In molecule (m)	**1**	**2**
1. Arc plasma	OO	OO
2. Residual liquid color	yellow	dark yellow

Note: OO = very stable

Additionally, various organic byproducts were also produced in the residual liquid as could be observed from the liquid colors as shown in both Table 5.4 and Figure 5.18(a). When arc plasma was terminated, anode tip

could be found as shown in Figure 5.18 (b) similar to alcohol systems. UV-VIS analysis of the obtained residual liquids from alkane system is shown in Figure 5.19. It could be observed that most of obtained byproducts are same while their quantities are different depend on carbon numbers in alkane molecule.

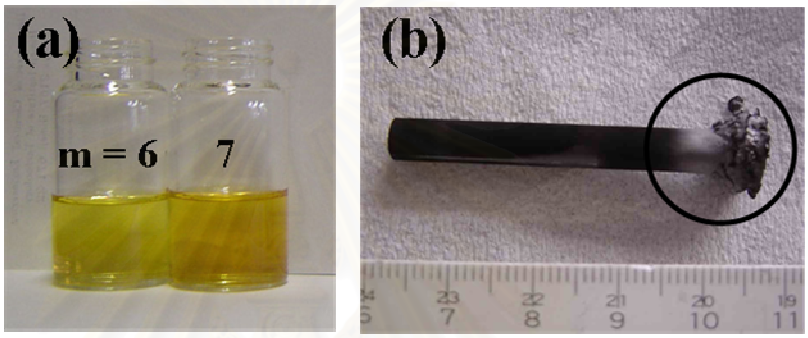

Figure 5.18 (a) Color of residual liquid by arc in alkane (C_mH_{2m+2}), and (b) Anode deposit after the arc discharge in Heptane (m=7)

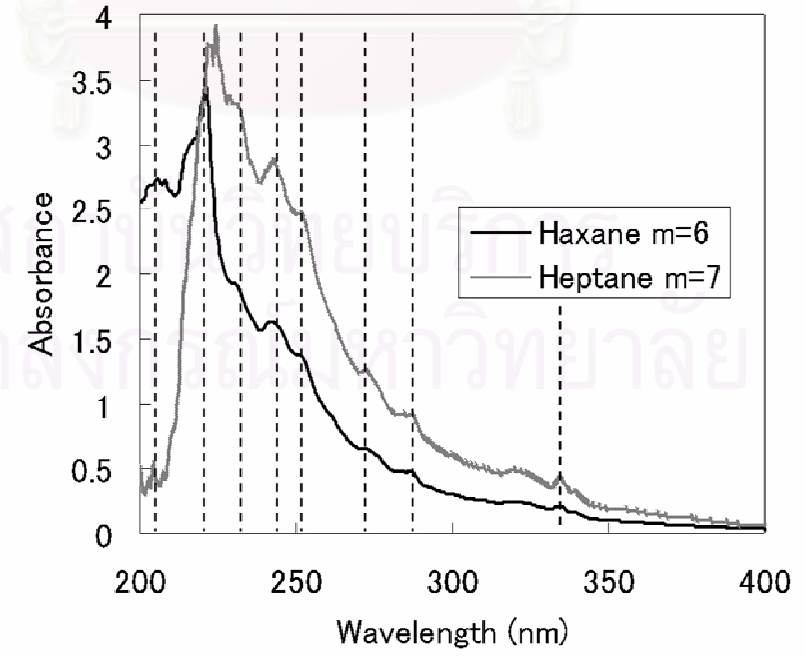

Figure 5.19 UV-VIS analysis of residual liquid in alkane cases

5.1.3.2 Microscopic analyses of the obtained products

Microscopic analyses from FESEM in Figure 5.20 reveals that synthesized product from cathode deposit by 'arc in alkane' are mainly CNPs which consist of MW-CNTs and multi-walled CNPs similar to alcohol systems. MW-CNTs with nominal diameter of 20 nm and length of 500 nm - 1 μm while shelled particles with diameter ca. 20-70 nm were observed in the concentration more than 50-60% based on random scanning. Moreover, other carbon structures including crystalline, amorphous carbons were also found. For sedimentary particles, majority of synthesized products are graphite and amorphous carbons. However, multi-shelled CNPs were also found in the concentration less than 5%. The main products in the anode tip are crystalline and disordered carbon while there are no CNPs similar to arc in alcohol systems.

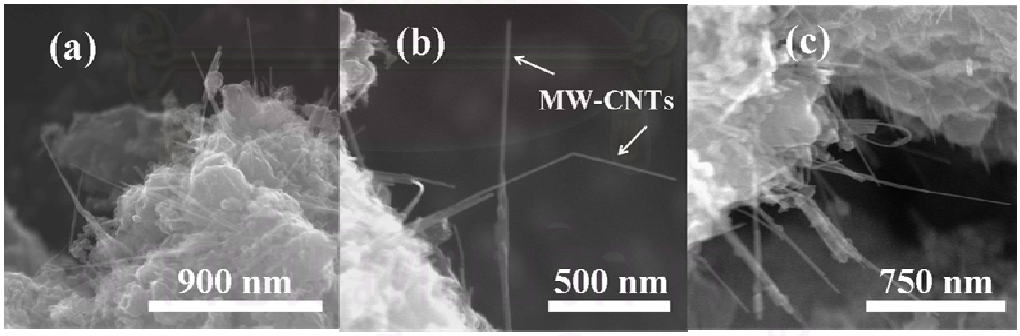

Figure 5.20 FESEM images of cathode deposit from
(a) Hexane (m=6) 100%, (b-c) Heptane (m=7) 100%

5.1.3.3 Production rate and yield

The production rate of collected products is shown in Figure 5.21. It could be suggested that when n-alkanes were employed, overall production

rate becomes higher than that of alcohol at the same carbon numbers because oxygen in alcohol would play a role as moderate oxidizer that would selectively remove amorphous carbon in the reaction field [34]. For the yield of cathode deposit, yield of hexane (m=6) and heptane (m=7) are 2.7 and 1.3, respectively. It should be noted that purity of CNPs-rich deposit in the case of alcohols becomes higher than that of alkane. Additionally, at the same carbon number, production yield of CNPs-rich product in alkane is lower than alcohol due to the effect of oxygen as discussed above.

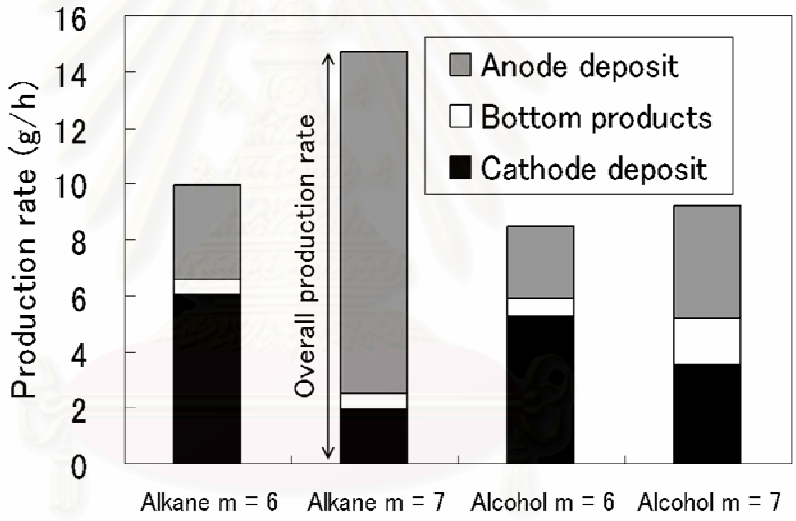

Figure 5.21 Influence of the number of carbon atoms in alkane molecule on the production rate of obtained products compared with alcohol systems

5.1.3.4 Particle size distribution

Typical average particle sizes of the CNPs-rich deposit obtained from DLS is shown in Figure 5.22.

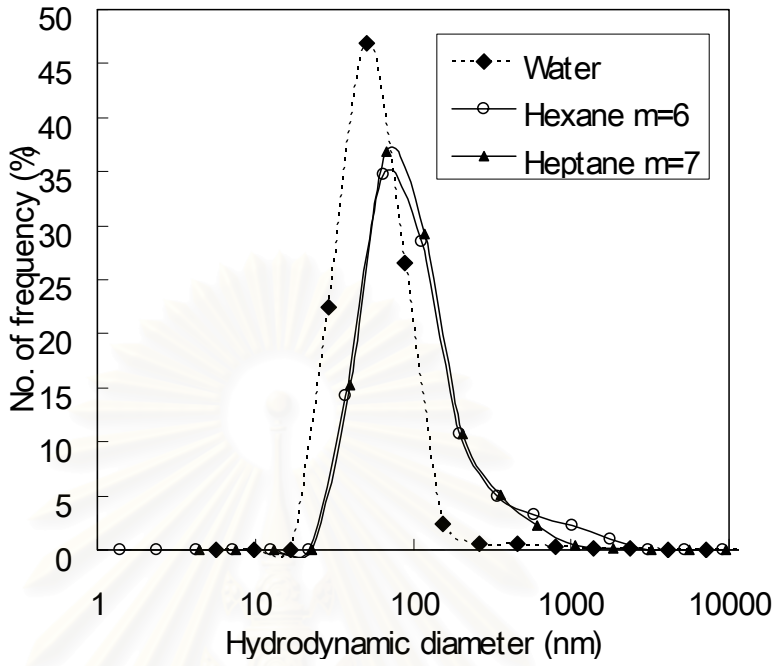

Figure 5.22 Influence of the number of carbon atoms in alkane molecules on the hydrodynamic diameter of CNPs-rich product

Figure 5.22 shows that mean hydrodynamic diameters from hexane (m=6), heptane (m=7), and water systems are 70, 68, and 51 nm, respectively. This presents that all mean hydrodynamic diameters when liquid alkanes were utilized are higher than that from water system as a result of selectivity of elongated structures to other polyhedral CNPs become higher than that from water similar to alcohol systems.

5.1.3.5 Raman spectroscopic analysis

Raman spectra reveal that G/D peak ratio from both hexane and heptane are about 1-1.2. Compared with alcohol systems, it could be observed that G/D ratios become lower than that from alcohol systems at the same

carbon numbers. It should be reminded that CNPs concentration is about 50-60% based on scanning observation. Other synthesized products are crystalline, amorphous carbon nanoclusters, and disordered carbon. However, among these products, disordered carbon quantities become higher than that of alcohol systems, resulting in a higher D-band peak was obtained.

5.1.3.6 Evaporation rate of the liquid

The evaporation rates of liquid are 6000, 4500, 890, and 400 ml/h for hexane (m=6), heptane (m=7), hexanol (m=6), and heptanol (m=7), respectively. This result indicates that evaporation rate become lower as the carbon numbers were increased. Additionally, the evaporation rate of alkane is higher than that of alcohol at the same carbon numbers. It is well known that in alcohol molecules, there are Van der Waal force in hydrophobic part and H-bond at the hydroxyl group. From this result, it can be concluded that Van der Waals interaction force of alcohol becomes stronger than that of alcohol system. This is an expected result due to the effect of vapor pressure difference.

5.1.4 Influence of aromatic liquid (C_6H_6-C_nH_{2n}, n=1,2)

5.1.4.1 Phenomena observed during the arc discharge

In this section, aromatic compounds were employed as liquid media to accommodate the plasma because there is no oxygen similar to n-alkane system including C to H ratio in aromatic molecule is higher than that in alkane molecule. Additionally, reactive double bond inside benzene ring could be expected to provide more preferable reaction to form CNPs. Therefore, aromatic compounds with typical formula (C_6H_6-C_nH_{2n}) such as Toluene (n=1) and Ethylbenzene (n=2) were used in this experiment.

During the arc discharge, arc plasma was not stable like other organic cases while high amount of white smoke could be observed continuously above the liquid surface. Based on this observation, it could be implied that benzene ring in these compounds have some effects to inhibit the plasma stability.

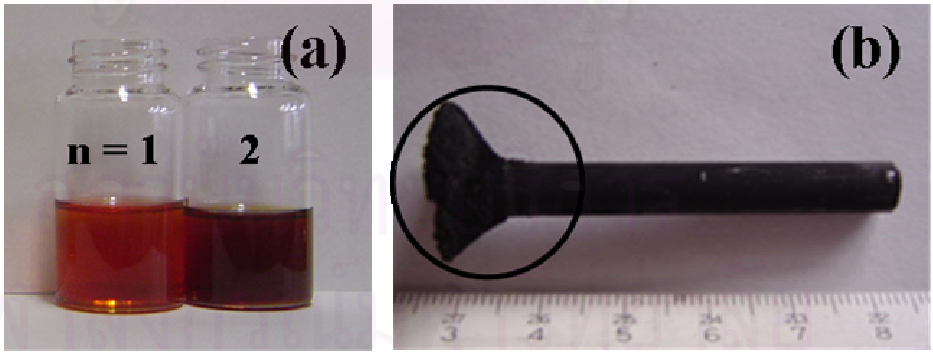

Figure 5.23 (a) Color of residual liquid by arc in aromatic ($C_6H_6CH_{2n}$), and (b) Anode deposit after the arc discharge in Toluene, n=1

Furthermore, three types of products can be synthesized similar to the alcohol and alkane systems. The anode deposit in bowl shape could be clearly

seen as shown in Figure 5.23. Such anode deposit shape has been already found in ‘arc in benzene’ which was reported by N. Sano [12].

Additionally, residual liquid color changed into black due to many fine particles suspended in the liquid. When these particles settled to the vessel bottom, residual liquid color of toluene and ethyl benzene systems turned to red and brown, respectively, as shown in Figure 5.23. For the absorption analysis, Figure 5.24 demonstrates that organic byproducts which are different from alcohol and alkane systems were also generated in the residual liquid.

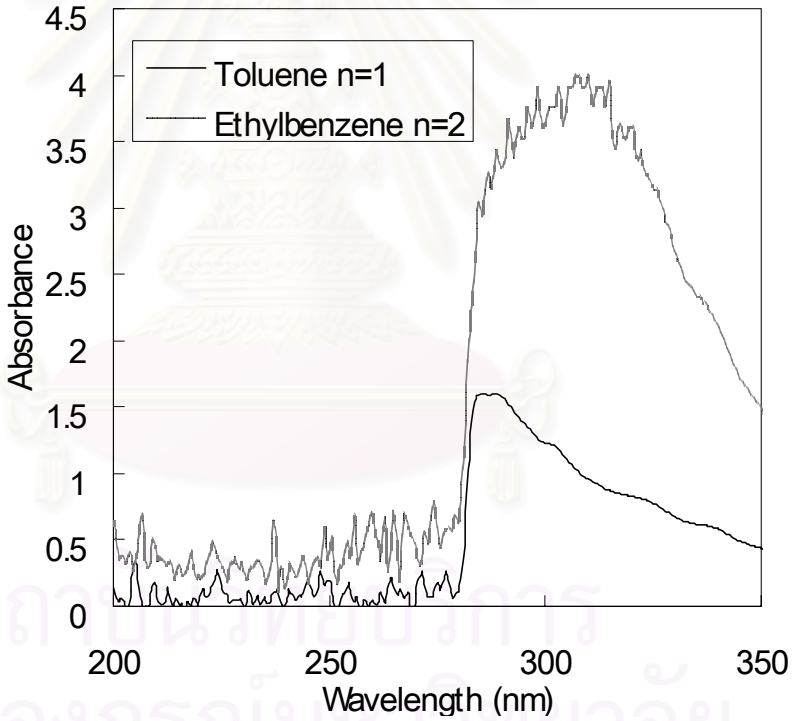

Figure 5.24 UV-VIS analysis of residual liquid in aromatic cases ($C_6H_6CH_{2n}$, n=1-2)

5.1.4.2 Microscopic analyses of the obtained products

Microscopic analyses of products obtained by arc in aromatic are conducted by TEM and shown in Figure 5.25. It reveals that synthesized products consist of MW-CNTs, multi-shelled CNPs (Figure 5.25a1), amorphous carbon (Fig. 5.25a2), and other disordered carbons could be observed in cathode tip from both Toluene (n=1) and Ethylbenzene (n=2) systems while disordered carbon are majority. It should be noted that CNPs become lower than 10% based on scanning observation. For the sedimentary particles and anode deposit, all are crystalline and disordered carbons while CNPs could not be observed.

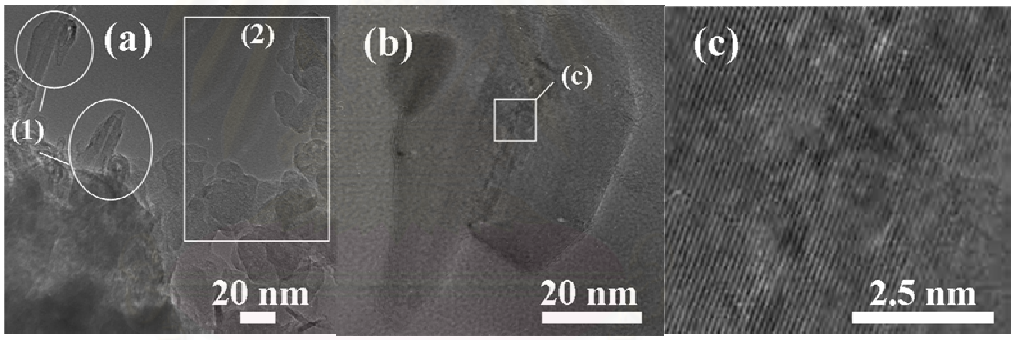

Figure 5.25 TEM images from arc in Toluene (cathode deposit), (a) overview of the obtained products, (b) MW-CNTs and shell-particles, and (c) high resolution of graphene sheets from (b)

5.1.4.3 Production rate and yield

The production rate of obtained products shown in Figure 5.26 suggests that majority of products are anode deposit which mainly consists of amorphous, crystalline and disordered carbons in high quantity. Additionally,

sedimentary particles could be also observed as majority synthesized product from aromatic systems.

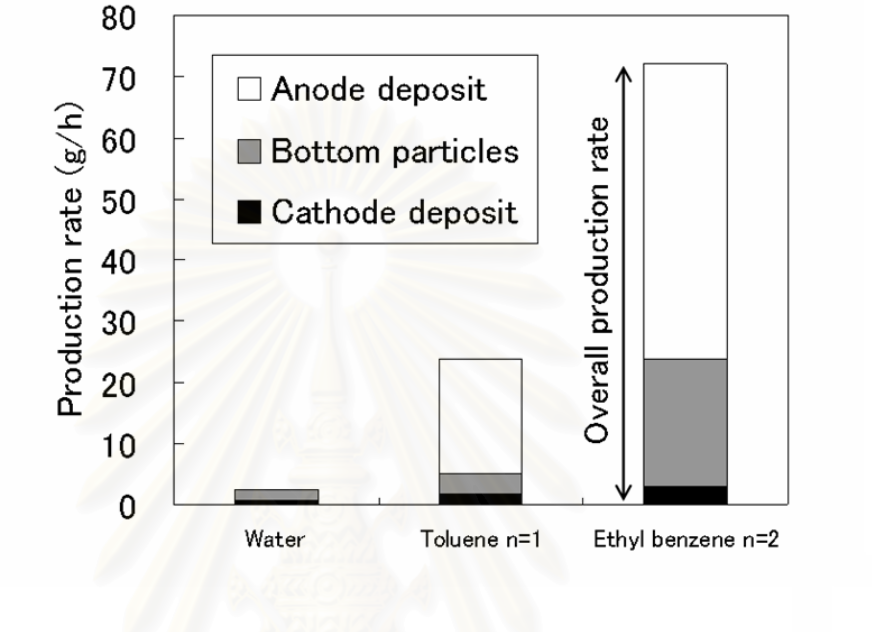

Figure 5.26 Influence of the aromatic compounds on the production rate of obtained products

From Figure 5.26, the quantity of cathode tip does not significantly differ in this graph as well as CNPs concentrations in that deposit are extremely low. Therefore, it could be concluded that aromatic compounds do not appropriate to supply carbon for CNPs synthesis.

5.1.4.4 Particle size distribution

Average particle size diameter obtained by DLS from H_2O, Toluene (n=1), and Ethylbenzene (n=2) are 51, 102, and 105 nm, respectively. These results are consistency with other organic cases that when organic liquid was

employed to supply carbon, elongated particle could be formed easier than short-shape particles. Additionally, it should be reminded that the obtained products are mainly disorder carbons which their sizes become larger than CNPs. This is the reason why DLS peak diameters obtained from aromatic systems become higher than that from H_2O system.

5.1.4.5 Raman spectroscopic analysis

The G/D ratio of the CNPs-rich product obtained from arc in H_2O, Toluene (n=1), and Ethylbenzene (n=2) are 3.9, 1.1, and 0.9 nm, respectively. These results reveal that D-peak increase when aromatic compounds were employed because high concentration of disordered carbons contain in the obtained products which is consistency with microscope analysis and particle size distribution as informed above.

Finally, types of products obtained from arc in organic compounds are summarized in Table 5.5 with the work about arc in benzene which was reported by N. Sano [12].

Table 5.5 Types of obtained products from arc in organic compounds

Type of products	Alcohol	Alkane	Aromatics compounds		
			Benzene	Toluene	Ethylbenzene
Cathode deposit	ABC	ABC	**BC***	ABC	ABC
Bottom particles	BC	BC	C	C	C
Anode deposit	C	C	C	C	C

A = MW-CNTs B = multi-shelled CNPs

C = other carbon structures (graphite, amorphous, and disordered carbons)

* No CNTs were found

Table 5.5 reveals that CNPs were not found in anode deposits for all conditions. For the bottom particles, multi-shelled particles could be observed only when alcohol and alkane were employed but their quantity were very rare (less than 5%) whereas there are no CNTs. On the tip of cathode, CNPs such as MW-CNTs and multi-shelled CNPs could be seen, but no CNTs could be observed from pure benzene system. This result confirms that CNTs which produced by arc in organic liquid used carbon atoms from alkyl groups as carbon source. Additionally, on the cathode deposite, purities of CNPs in alcohols and alkanes systems become higher than that of aromatic compounds. Averagely speaking, purity for alcohols and alkanes cases is about 70% and purity for aromatics cases is less than 30% based on the scanning observation.

5.1.5 Influence of addition of surfactant (Monoolein)

5.1.5.1 Phenomena observed during the arc discharge

In the previous investigations, pure organic liquids were employed as liquid media to supply additional carbon into plasma zone besides anode electrode. However, those organic liquids have high vapor pressures which cause easily to be explosion. Therefore, in this section, surfactant was utilized to mix the organic compound and water together. Lower vapor pressure of organic liquids could be expected as an alternative way which is much safer than using pure organic compound as a liquid for arc discharge. To achieve this, n-hexane (C_6H_{14}) was utilized as organic liquid since n-hexane has vapor pressure higher than alcohol and aromatic at the same carbon number in the molecule. Additionally, n-hexane cannot solute in water, leading to observe the effect of surfactant more clearly. For the surfactant, monoolein ($C_{17}H_{35}COO\text{-}\ CH_2CH(OH)CH_2OH$) was chosen to be the surfactant used in this case because this surfactant is a non-ionic type which does not have the electrical effect on the carbon radical in the reaction field.

During the arc discharge, arc plasma was very stable. The liquid before the arc discharge was white and became more transparent when the arc discharge was started. After plasma was terminated, two types of products could be found. One was the cathode deposit and another was the bottom products. It should be reminded that in the conventional arc in water, floating particles could be also observed. Based on this phenomenon, it could be implied that surfactant can help to reduce density of the liquid.

5.1.5.2 Microscopic analyses of the obtained products

As mentioned above, only cathode deposit and sediment particles were found as the obtained products. TEM images of cathode deposit are shown in Figure 5.27. It could be seen that CNPs consist of multi-shelled particles, MW-CNTs and carbon nano-onions could be observed. Additionally, it should be noted that concentration of these nano-carbons become higher than 80% based on random observation from TEM. Figure 5.27a-b show typical TEM images of the synthesized CNPs in the cathode tip as well as Figure 5.27c also shows the high magnification of carbon nano-onions which have graphene sheets more than 20 layers in the cathode deposite. Among the obtained CNPs, the quantities of multi-shelled CNPs are higher than MW-CNTs and carbon nano-onions, respectively. Furthermore, amorphous carbon clusters and crystalline could be also found with low concentration in the cathode deposit.

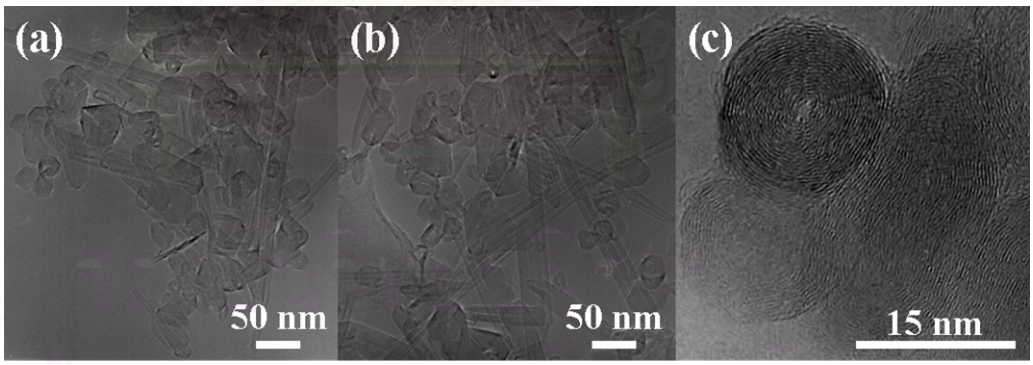

Figure 5.27 TEM images of cathode deposit obtained from arc in surfactant, (a-b) 0.3 g olein, and (c) 3 g olein

For the bottom particles, it could be seen from Figure 5.28a that various types of particles were produced. In the bottom-1, CNPs including multi-shelled CNPs and MW-CNTs could be observed with concentration

about 20% if 0.003 g of olein was used. With the increasing amount of olein to 3 g, concentration of obtained CNPs becomes lower to 10%. In the bottom-2, crystalline and disordered carbon could be seen as a major product. Next, Figure 5.28b shows the high resolution of graphene sheets of obtained crystalline in two directions from the synthesized product.

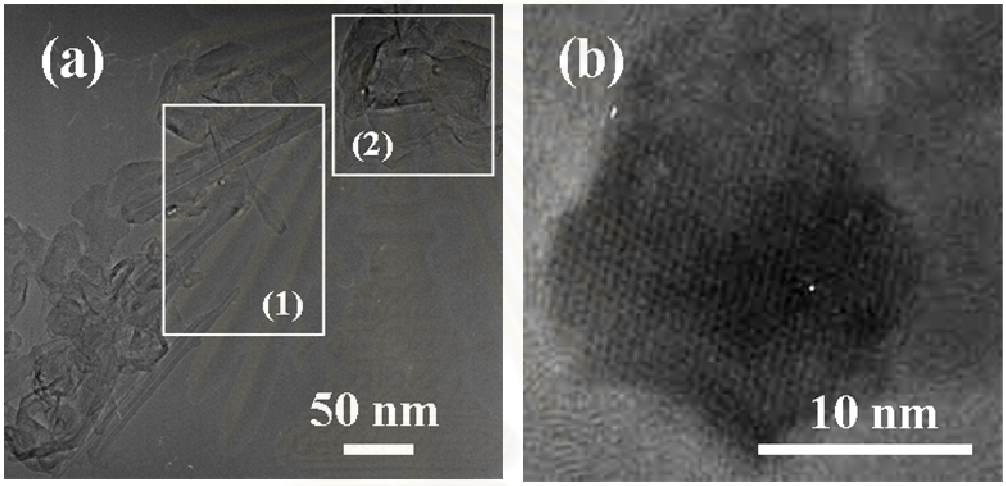

Figure 5.28 TEM images of bottom particles obtained from arc in surfactant, (a) 0.003 g olein, and (b) 3 g olein

5.1.5.3 Production rate and yield

The production rates of obtained particles are shown in Figure 5.29 as a function of the amount of surfactant. A cathode tip formation rate becomes higher as the amount of monoolein is increased within a lower quantity of surfactant region (less than 0.01 g of surfactant) as well as there is a highest formation rate when 0.3 g of monoolein was employed. After this point, formation rate become lower with the increasing amount of surfactant. For the bottom particles, the formation rate becomes lower when the amount of

surfactant is increased. The overall production rate becomes higher until at 0.03 g of monoolein, after this point, production rate decrease with the increasing of amount of monoolein.

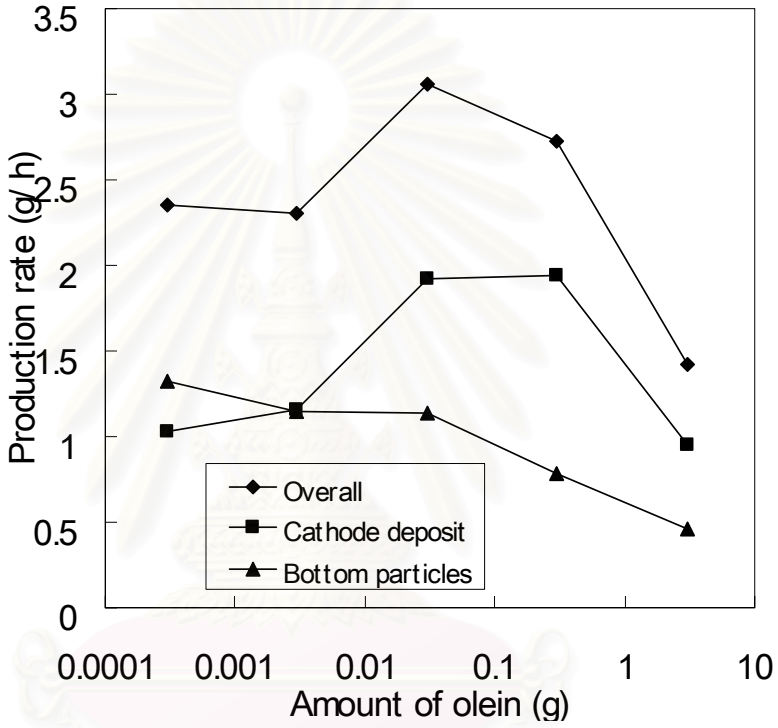

Figure 5.29 Influence of the amount of surfactant (olein) on the production rate of obtained products

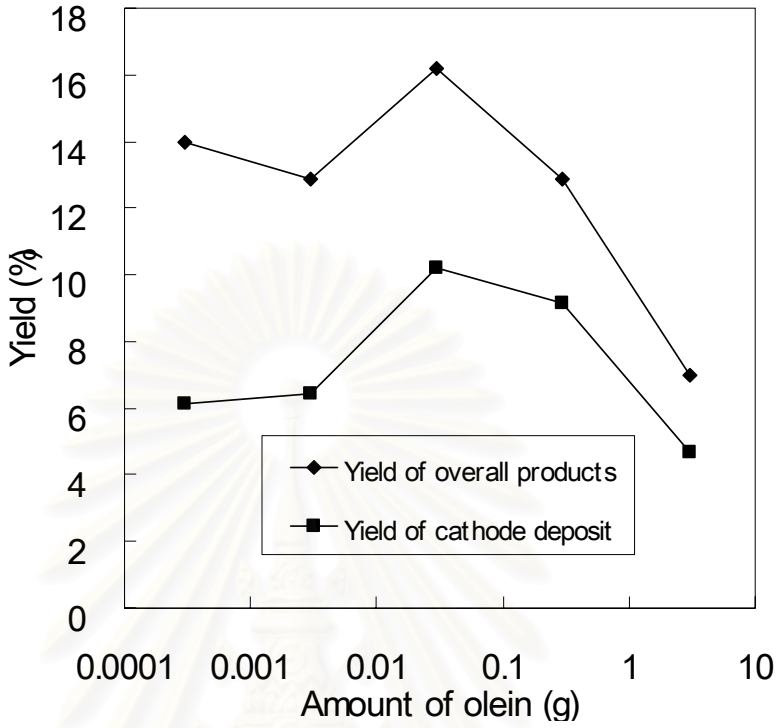

Figure 5.30 Influence of the amount of surfactant (monoolein) on the yield of obtained products

The production yield of overall products and CNPs-rich products (cathode tip) are shown in Figure 5.30. Assuming, the condition when 0.0001 g of monoolein was employed is similar to pure water system because the amount of n-hexane is extremely diluted. It could be clearly seen from Figure 5.30 that within a range of 0.01-0.1 g of monoolein, production yield becomes higher than that from arc in water. Furthermore, both yields reach to the highest point when 0.03 g of monoolein was employed. Based on this investigation, it can be summarized that the appropriate quantity amount of monoolein to synthesize CNPs is in a range of 0.01-0.1 g.

5.1.5.4 Particle size distribution

Typical particle sizes of CNPs-rich products evaluated by DLS are shown in Figure 5.31. This figure demonstrated that the hydrodynamic diameters of products are ranging in 50-130 nm which are higher than that from arc in pure water. Based on this result, it could be implied that the surfactant would catch organic compound molecule into the water, resulting in the increase of carbon atoms as additional carbon source which is not only from organic compound but also from the surfactant in the reaction field. Then the elongated particles could be easily produced due to the continuously supplied of carbon to the reaction field.

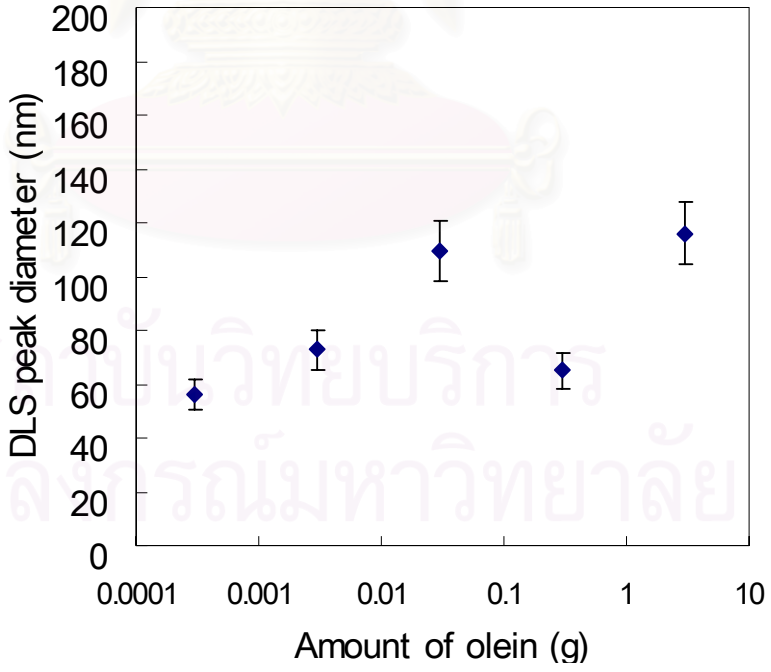

Figure 5.31 Influence of amount of surfactant on the hydrodynamic diameter of CNPs-rich product

5.1.5.5 Raman spectroscopic analysis

The G/D ratios obtained from the Raman analyses are shown in Figure 5.32. This presents that G/D ratio become highest when 0.3 g of monoolein is used. Additionally, the G/D ratio of the CNP-rich deviates within a range of 4.3-7.5.

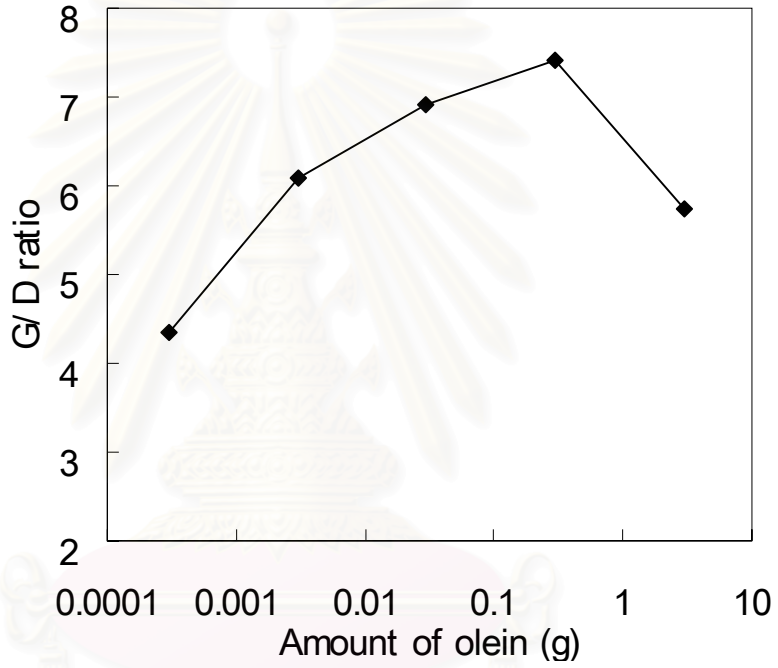

Figure 5.32 Influence of amount of surfactant on the G/D ratio of the CNPs-rich product

5.1.5.6 The measurement of vapor pressure in the sample

The vapor pressure of the organic compound (n-hexane) in liquid media in each condition was experimentally estimated from the integrated area under the n-hexane peak obtained from gas chromatography (GC) and then compared with the integrated area when pure n-hexane was employed. It is well known that vapor pressure of n-hexane in each temperature could be also

theoretically estimated from Antoine laws. From these considerations, vapor pressure in each condition could be roughly calculated. The integrated peak area of the n-hexane in the liquid media are shown in Figure 5.33

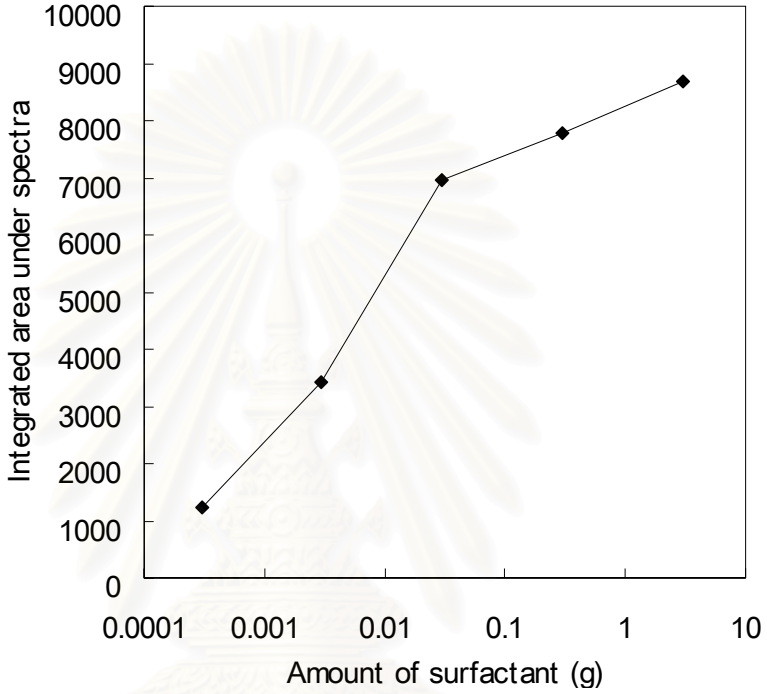

Figure 5.33 The relationship of integrated area under spectra from GC as a function of amount of surfactant

Figure 5.33 demonstrates that integrated area becomes higher with the increasing amount of surfactant. Based on this result, it could be confirmed that when more surfactant was utilized, the more n-hexane could disperse into the system.

Table 5.6 Influence of amount of surfactant on the vapor pressure of n-hexane

Amount of olein (g)	Integrated area	Vapor pressure of n-hexane at 13 ^{o}C (Pa)
Pure Hexane	13356593.0	11704.7
3 g	8685.2	7.6
0.3 g	7794.0	6.8
0.03 g	6962.6	6.1
0.003 g	3412.2	3.0
0.0003 g	1236.0	1.1

The vapor pressure of n-hexane in the liquid was summarized in Table 5.6. This presents that the use of surfactant could decrease the vapor pressure of n-hexane about 1,500-10,000 times compared with that of pure n-hexane system. The lower vapor pressure of n-hexane could be obtained as an alternative way which is more safety than using pure organic liquid. Therefore, the use of surfactant to mix organic liquid into water is a currently attempt technique to increase carbon atom into the reaction field.

Table 5.7 Purity of products, production rate of cathode deposit, and vapor pressure of n-hexane when pure n-hexane, pure water, and surfactant were used as liquid media for arcing

Condition	CNPs at cathode deposit (%Purity)	Production rate of cathode deposit (g/h)	Vapor pressure of n-hexane at 13 ^{o}C (Pa)
Pure n-hexane	>70 %	6.1	11704.7
Water + n-hexane	70-80%	1-2	1-8
Pure Water	60-70%	0.8	0

Table 5.7 compares the purity of CNPs-rich products, production rate of cathode deposit, and vapor pressure of n-hexane when pure n-hexane, pure water, and n-hexane mixed with water by surfactant were employed. It could be seen that both pure n-hexane and surfactant were used, the purity of CNPs were much more than 70% which was higher than that from pure water. Moreover, production rate of cathode tip in surfactant system is broader than that from pure water, but it become lower than that from pure n-hexane. This is because additional carbon atom from pure n-hexane is higher than surfactant, and in the case of pure water, no extra carbon from the liquid supplied to the reaction zone. Finally, the vapor pressure in surfactant case was much lower than that in pure n-hexane. Therefore, gas purging system is not necessary when surfactant was utilized, resulting in the setting cost would be lower. In summary, arc in water with surfactant is an alternative technique to increase yield and production rate of obtained particles.

5.2 Influence of inorganic compounds

5.2.1 Influence of Na_2CO_3 solution

5.2.1.1 Observed phenomena during the arc discharge

Since Na_2CO_3 contain some certain amount of carbon atoms in their molecule similar to organic compound, it is expected that using a Na_2CO_3 solution to accommodate the arc plasma might help provide additional carbon atoms to engage in CNPs synthesizing reaction. Additionally, an existing of cations in reaction zone is also expected to play a role as catalyst to enhance formation of CNPs.

In this experiment, Na_2CO_3 solutions which their concentrations were varying from 0.01 to 1.0 M were employed as liquid media for arcing. When the arc plasma was started, there were many fine bubbles emerging from both electrodes, and then there were some black particles as well as gas bubbles emerging from the reaction field. After terminated arc plasma, there were many fine particles suspended in the solution. The color of the solution was yellow when the concentration of Na_2CO_3 was higher than 0.1 M. Arc plasma tended to be unstable when increasing the concentration of Na_2CO_3. For the obtained products, there was deposition only on the cathode while anode was consumed steadily during the arc discharge. Besides the cathode deposit, there were some sediment particles at the bottom of vessel, which they are in the form of small circular flakes.

5.2.1.2 Microscopic analyses of the obtained products

Typical microscopic images of obtained particles from arc in Na_2CO_3 solution of 0.1 M are shown in Figure 5.34. From Figure 5.34a, it could be seen that the synthesized products are mixtures of CNPs with different morphology similar to those of previous investigations. These CNPs are mainly composed of entangling multi-walled carbon nanotubes (MW-CNTs) and polyhedral crystalline carbon shells as well as some of amorphous carbon fine particles. Based on the scanning observation, it should be noted that concentration of CNPs seemed to be 60-70% in this condition. It is reasonable that these different nanoparticles could be synthesized by the different conditions co-existing in the reaction zone and then mixed up by agitation due to bubbles emerging at vicinity of the electrodes.

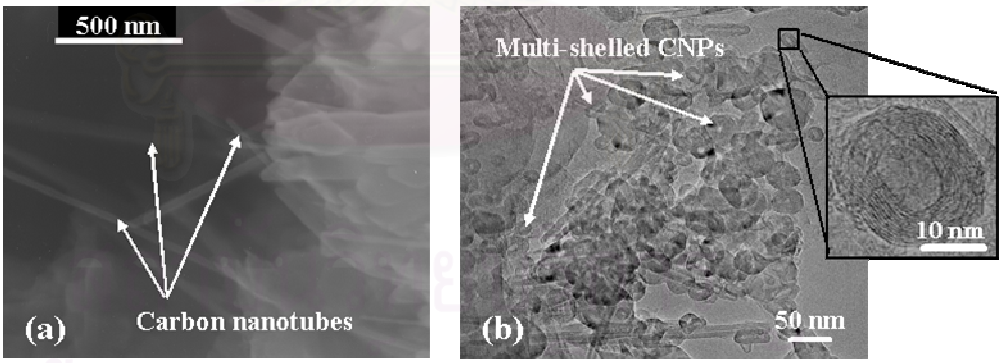

Figure 5.34 Microscope analyses from cathode deposit by arc in Na_2CO_3 0.1 M, (a) FESEM image of MW-CNTs, (b) TEM image of mixtures of CNPs

Similarly, consistent images obtained from Transmission Electron Microscopic analysis in Figure 5.34b shows the clear appearance of CNP

mixtures obtained from the aqueous solution of 0.1 M Na_2CO_3. This higher magnification image of TEM shows that the MW-CNTs have diameter of 30-40 nm with length of ca. 700 nm while the nearly spherical polyhedral particles have the size range of 20-120 nm. Compared with previous investigations, it could be observed that the walls of CNPs synthesized in aqueous solution was comparatively composed of some defects different from that of pure de-ionized water. There were some amorphous carbons with irregular morphology existing in the synthesized products. However, their size distribution is much broader than that of crystalline polyhedral particles.

Nevertheless, when concentration of Na_2CO_3 reachs higher than 0.1 M, the concentration of synthesized CNPs become lower. For example, in the case of 0.5 and 1.0 M of Na_2CO_3 solution, concentrations of obtained CNPs were approximately 40% and 25%, respectively. According to the results, it could be implied that existence of ions in a few amount at arc discharge zone would play a role as catalyst to enhance formation of elongated MW-CNTs. Nevertheless, no metal or metallic compounds encapsulated in the obtained CNPs could be observed from TEM images of analyzed specimens.

5.2.1.3 Production rate and yield

The production rate and yield of the obtained products are shown in Fig. 5.35 as a function of the concentration of Na_2CO_3.

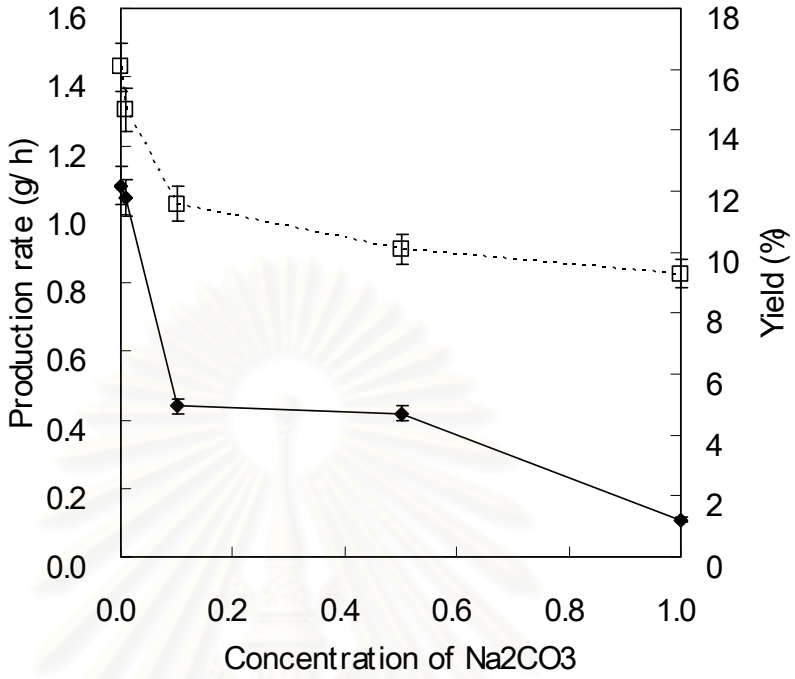

Figure 5.35 Influence of the concentration of Na_2CO_3 on the yield and production rate of obtained products

It could be seen from Figure 5.35 that both yield and production rate become lower with the increasing concentration of Na_2CO_3. It should be reminded that arc plasma became less stable when increasing the concentration of Na_2CO_3. Based on this result, it could be implied that high concentration of ions had electrical effect with the carbon radical at the plasma zone which would disturb the formation of CNPs. However, it must be noted that the maximum concentration at which arc plasma could be maintained is approximately 2.09 M (the saturated condition of Na_2CO_3 at 25 ^{o}C is 3.45 M).

5.2.1.4 Particle size distribution

Typical particle sizes evaluated by DLS shown in Figure 5.36 had been employed for statistically determining size distribution of specimens obtained from the arc discharge in Na_2CO_3 solution.

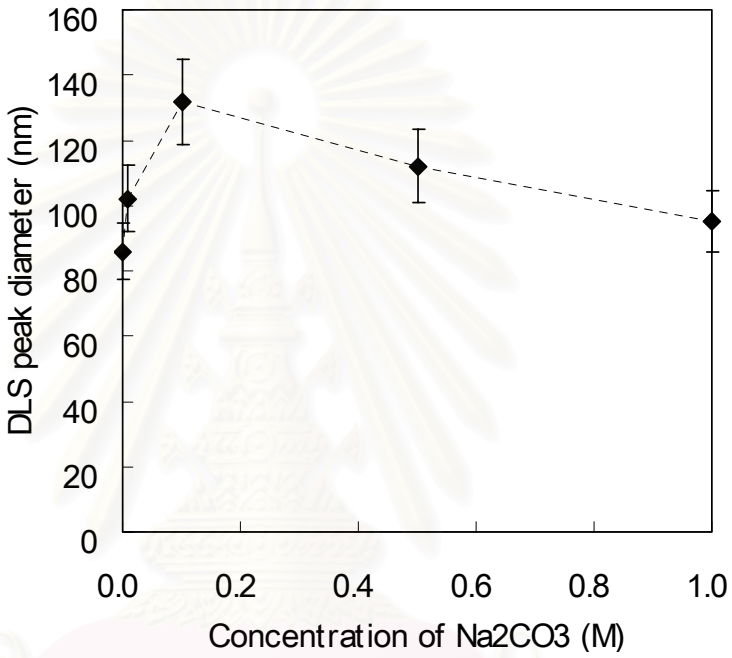

Figure 5.36 Influence of the concentration of Na_2CO_3 on the hydrodynamic diameter of CNPs-rich product

Figure 5.36 shows that addition of Na_2CO_3 into de-ionized water in the proper amount give rise to longer hydrodynamic diameter of 90-140 nm compared with that of pure de-ionized water (ca. 85 nm.). This is consistent with the microscopic evidence shown in Figure 5.36.

5.2.1.5 Raman spectroscopy

The intensity ratio of G-band to D-band (G/D ratio) in the spectrum of the as-produced CNPs is shown in Figure 5.37. This indicates that the obtained CNPs have well graphitized structure at concentration 0.1 M which is also consistent with microscopic analyses and DLS results.

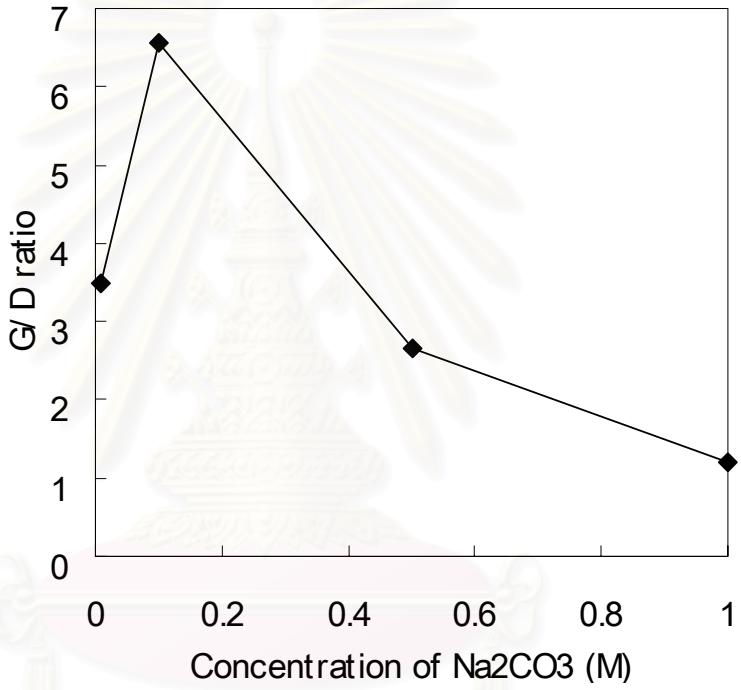

Figure 5.37 Influence of the concentration of Na_2CO_3 on the G/D ratio of CNPs-rich product

Based on all analysis, it could be summarized that the appropriate concentration to synthesize CNPs is 0.1 M of Na_2CO_3 solution.

5.2.2 Influence of transition metal salt solution ($NiSO_4$, $CoSO_4$ and $FeSO_4$)

5.2.2.1 Phenomena observed during the arc discharge

In this section liquid media from metal salt solution was employed for arc discharge. It was reported that these metal would play a role as catalyst to increase production yield and formation rate of CNPs-rich products. Therefore, $NiSO_4$, $CoSO_4$, and $FeSO_4$ were utilized in this work.

With using $NiSO_4$ solution, there are many fine bubbles emerging from cathode electrode. The color of the liquid before arcing was green and then solution turned into dark green due to the dispersed and sediment particles. Three types of products could be observed after the arc discharge: cathode deposit, floating particles, and sediment particles. The amounts of floating particles become lower with the increasing concentration of $NiSO_4$. The arc stability was similar to Na_2CO_3 system that arc plasma became unstable with an increase of $NiSO_4$ concentration but when low concentration of $NiSO_4$ (0.02 M) was employed, arc plasma was very stable. Additionally, there is odor like S compounds during the experiment. Maybe, this compound is SO_2 that need more analysis in the next work.

When $CoSO_4$ solution was utilized, similar to $NiSO_4$ system, many fine bubbles emerging from cathode electrode could be also observed. Liquid color before arcing was red and then solution turned into dark red because of the suspended and bottom carbon powders. Three types of products could be observed including cathode tip, floating particles, and sedimentary particles. Majority of products are the particles at vessel bottoms which are gray particles mixed with black fine particles. These particles were expected as Co

compounds which will be analyzed by XRD later. The amount of floating particles becomes lower with the increasing concentration of $CoSO_4$. For the arc stability, arc plasma became unstable with the increasing the concentration of $CoSO_4$. Inversely, at the low concentration of $CoSO_4$ (0.02 M), arc plasma was very stable.

In the case of $FeSO_4$ solution, similar to the previous investigations, there are many fine bubbles emerging from cathode side. The color of the liquid before arcing was light yellow and then solution changed into yellow the dispersed and sediment particles. Three types of products could be observed. The amount of floating particles becomes lower with the increasing $FeSO_4$ concentration. The more unstable arc plasma could be obtained with the increasing concentration of $FeSO_4$, but in the low concentration of $FeSO_4$ (0.02 M), arc plasma was very stable.

5.2.2.2 Microscope analyses of the obtained products

First, it should be reminded that three types of products could be seen when plasma was terminated, but during the arc discharge, some of cathode deposit peeled away and mixed with the sedimentary product due to the pressure from the arc plasma. It is very hard to separate these products for the reason that the quantity of bottom products is very much. Therefore, the analyses of bottom products mean the mixtures of sedimentary particles and the cathode deposit.

When $NiSO_4$ solution was employed, typical images from bottom products obtained by TEM are shown in Figure 5.38. It could be observed that

the synthesized products are mixtures of CNPs and Ni compounds with different morphology. The CNPs consist of multi-walled carbon nanotubes (MW-CNTs) and polyhedral crystalline carbon shells. These figures demonstrate that the nearly spherical polyhedral particles with their size range of 20-70 nm while the MW-CNTs have diameter of 10-20 nm with the length of 200-300 nm could be seen. The Ni compounds have size range from 20 nm to more than 1 micron as well as there is various shapes such as needle shape, spherical and polyhedral particles. Species of Ni compounds would be investigated by XRD which will be discussed later. For the obtained CNPs, it is noteworthy that the amount of CNPs seemed to be 60-70% when $NiSO_4$ 0.02 M solution was employed and the concentration of CNPs become lower with the increasing concentration of solution. The ratio of shelled particles and elongated nano-carbons was 7:3 in $NiSO_4$ 0.02 M condition based on random scanning obtained from TEM. Furthermore, there were some amorphous carbon and graphite with irregular morphology existing in the synthesized products. However, their size distributions are much broader than that of multi-shelled particles.

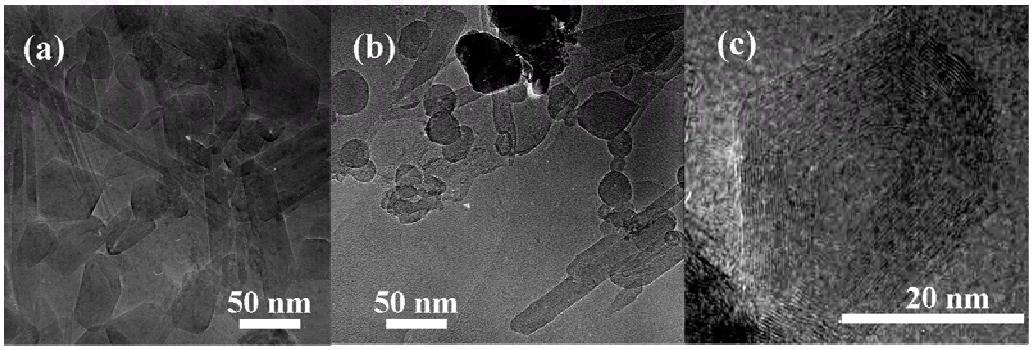

Figure 5.38 TEM images of bottom particles from

(a, b) $NiSO_4$ 0.02 M, and (c) $NiSO_4$ 0.2 M

For the floating particles, Figure 5.39a presents that most are graphite and amorphous carbon. It could be found multi-shelled CNPs only a little amount as well as the concentration of CNPs seemed less than 10%. The Ni compound such as NiO and Ni_xS_y which have needle, polyhedral shapes can be also found in the floating powder. Nevertheless, no metal or metallic compounds encapsulated in the obtained CNPs could be observed from TEM images of analyzed specimens.

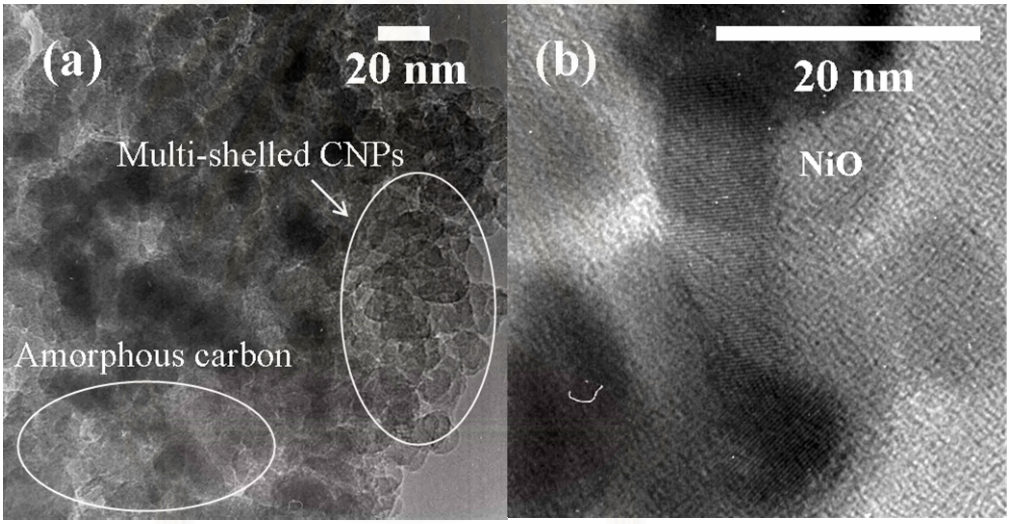

Figure 5.39 TEM images of floating particles from (a) $NiSO_4$ 0.02 M, and (b) $NiSO_4$ 0.1 M

With using $CoSO_4$ solution, TEM images from bottom products shown in Figure 5.40 presents that CNPs mixtures including Co compounds with different morphology could be mainly found as the synthesized products similar to $NiSO_4$ systems. From Figure 5.40a in the bottom-1, the CNPs consist of multi-walled carbon nanotubes (MW-CNTs) and polyhedral

crystalline carbon shells. The shelled particles ranging of 20-60 nm in size and MW-CNTs have diameter of 10-20 nm with the length of 100-600 nm could be obtained. In bottom-2, Co compounds have size range from 30 nm to more than 1 micron and there are various shapes such as needle shape, spherical and polyhedral particles. The concentration of Co compounds become higher when high quantity of $CoSO_4$ was used as shown in Figure 5.40. For the obtained CNPs, it is noteworthy that concentration of CNPs seemed obviously about 60-70% when $CoSO_4$ 0.02 M solution was employed. Furthermore, CNPs concentration becomes lower with an increase of concentration of solution.

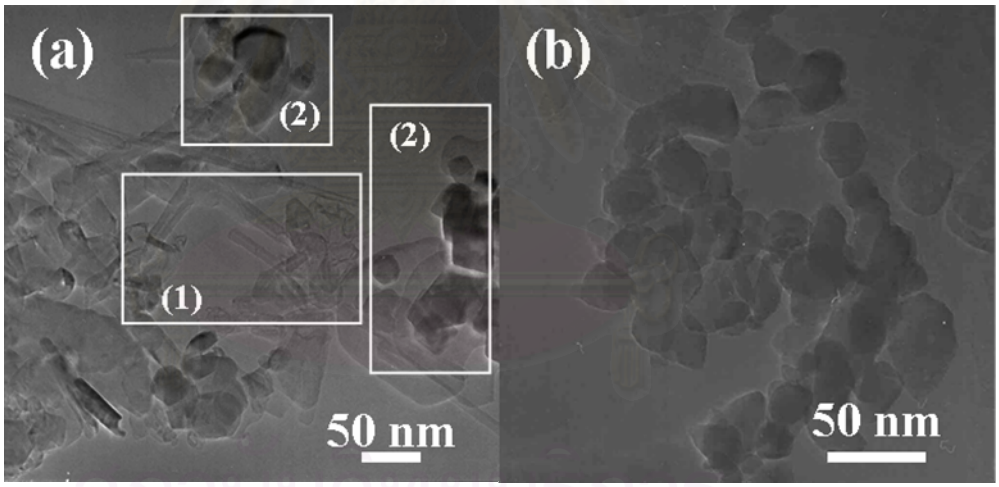

Figure 5.40 TEM images of bottom particles obtained from (a) $CoSO_4$ 0.2 M, and (b) $CoSO_4$ 0.3 M

In this condition, nearly spherical shape of Co compound was mainly found as obtained products. The ratio of shelled particles and elongated nano-carbons was 3:1 in $CoSO_4$ 0.02 M conditions observed by TEM. Additionally, there were some amorphous and crystalline carbons with irregular morphology

existing in the synthesized products. However, their average hydrodynamic diameters are much broader than that of multi-shelled particles. Interestingly, there were no metal or metallic compounds encapsulated in the obtained CNPs.

For the particles at liquid surface, Figure 5.41 presents that majority of products consist of crystalline and amorphous carbon structures. It could be found multi-shelled CNPs only a little amount as well as CNPs concentration become lower than 10%. The Ni compounds which have needle form as shown in Figure 5.41a, and the polyhedral shapes in Figure 5.41b can be also found in the floating powder. Nevertheless, no metal or metallic compounds encapsulated in the obtained CNPs could be observed from TEM images of analyzed specimens.

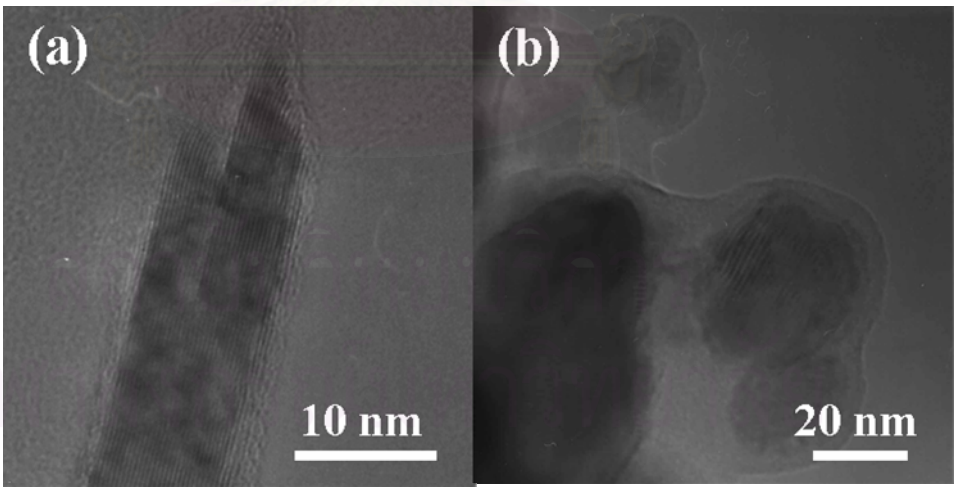

Figure 5.41 TEM images of floating particles from $CoSO_4$ 0.02 M

In the case of $FeSO_4$, TEM images from bottom products shown in Fig. 5.42a presents that synthesized products are mixtures of CNPs and Fe compounds with different morphology similar to the two previous cases.

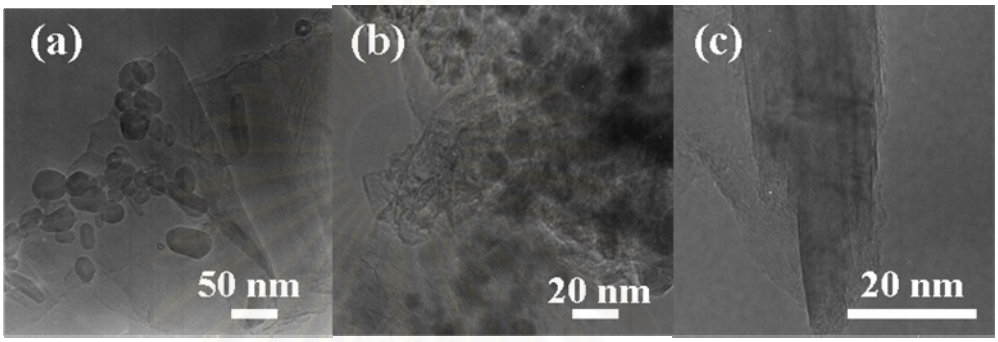

Figure 5.42 TEM images from (a) $FeSO_4$ 0.02 M bottom particles, (b) $FeSO_4$ 0.3 M bottom particles, and (c) $FeSO_4$ 0.02 M floating particles

From Figure 5.42a, CNPs consist of multi-walled carbon nanotubes (MW-CNTs) and polyhedral crystalline carbon shells. The multi-shelled CNPs have size range of 20-70 nm while the MW-CNTs have diameter of 10-20 nm with the length of 100-600 nm. Fe compounds have size range from 30 nm to more than 1 micron.. For the obtained CNPs, it is noteworthy that the amount of CNPs seemed to be 60-70% when $FeSO_4$ 0.02 M solution was employed and the concentration of CNPs will decrease with increasing concentration of solution which is similar to the previous investigation. The concentration of Fe compounds seemed increase when high amount of $FeSO_4$ was used as shown in Figure 5.42b. The ratio of shelled particles and elongated nano-carbons was 3:1 in $FeSO_4$ 0.02 M conditions based on scanning observation by TEM. Additionally, some amorphous and crystalline carbon could be generated in

the prepared products. However, their size distributions are much broader than that of multi-shelled particles. Interestingly, there were no metal or metallic compounds encapsulated in the obtained CNPs. For the floating particles, the main product was Fe compounds which had various shapes such as needle and spherical shape. The amorphous carbon and graphite can be also found as well as there were no CNPs in the floating powder.

5.2.2.3 Percentage of metal in the samples

The percentage of metal in the synthesized products in each condition was evaluated by burning known weight of samples in the furnace at 700 ^{o}C for 10 hr and then measuring the weight of residual product which were oxide of their metals. Assuming that all of carbons in the samples were completely burning then the percentage of metal can be obtained. Figure 5.43 indicates that percentage of metal in the obtained sample become higher with the increasing concentration of solution. The increase of metal percentage in the cases of Ni and Fe seemed linearity while the increasing of Co was logarithm correlation. The maximum percentage of Ni and Fe were less than 10% when 0.3 M of solution was employed. However, the maximum percentage in the case of Co was approximately 95%. This is because by-products from the electrolysis reaction when CoSO4 was employed also contaminated in the sample which could not be found with using $FeSO_4$ and $NiSO_4$ system due to the difference of half-cell value (E^{o}) in each system.

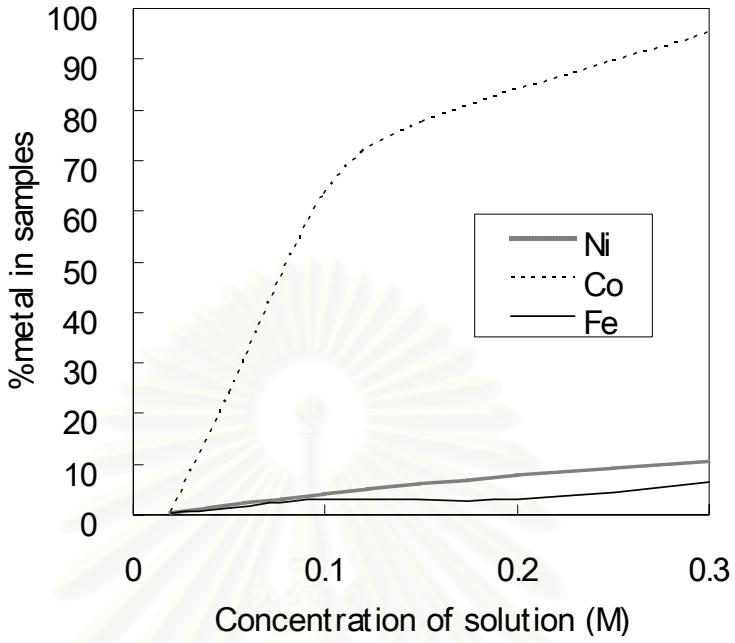

Figure 5.43 Influence of concentration of solution on the percentage of metal in the samples

5.2.2.4 X-Ray Diffraction (XRD)

The XRD patterns obtained from arc in $NiSO_4$ solution are summarized in Figure 5.44. It could be seen from this Figure that various species of Ni compounds were detected in the samples such as NiO, NiS, and Ni_3S_2. From this figure, NiO can found in all conditions. Interestingly, at the concentration of $NiSO_4$ less than 0.1M, there were no Ni_xS_y. When increasing the concentration of NiSO4 to 0.2 M, Ni_3S_2 can be found. In addition, in the case of $NiSO_4$ 0.3 M, NiS can be observed while Ni_3S_2 cannot be seen. It can be concluded that concentration of $NiSO_4$ has some effect on the formation of Ni_xS_y compounds.

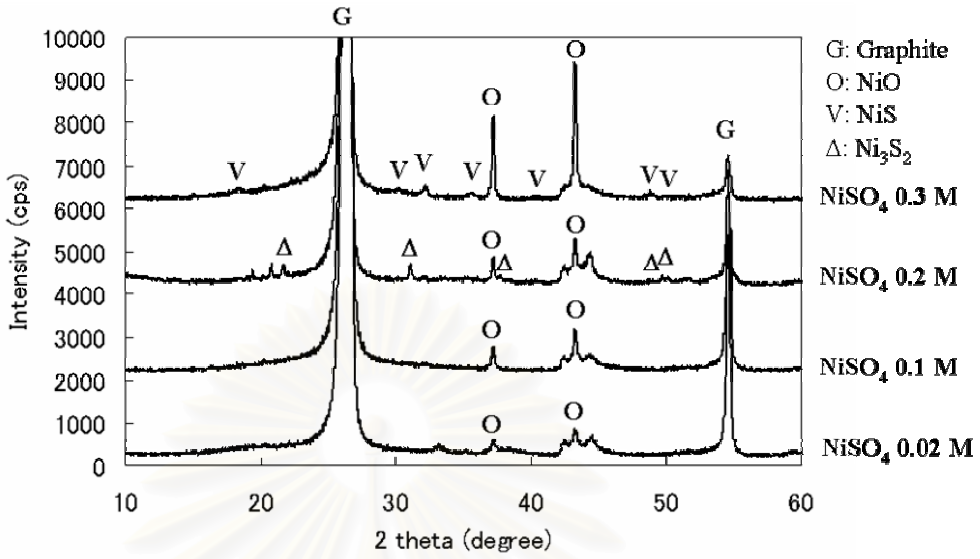

Figure 5.44 XRD patterns obtained from arc in $NiSO_4$ solution

In the case of $CoSO_4$, pure Cu, CO_3O_4, and $Co(OH)_2$ could be found in the synthesized products conducted by XRD as shown in Figure 5.45. It should be reminded that the percentage of Co in the samples were higher than that in Ni and Fe solution at the same concentration. When the concentration was less than 0.1M, only pure Co can be found as a contaminating product in the sample. When the concentration higher than 0.1 M, Co_3O_4 and $Co(OH)_2$ were found in the synthesized products. Then the concentration of $CoSO_4$ can be selectively formed the Co compounds in the obtained product similar to $NiSO_4$ cases. However, there was no S compound in the sample like $NiSO_4$ cases.

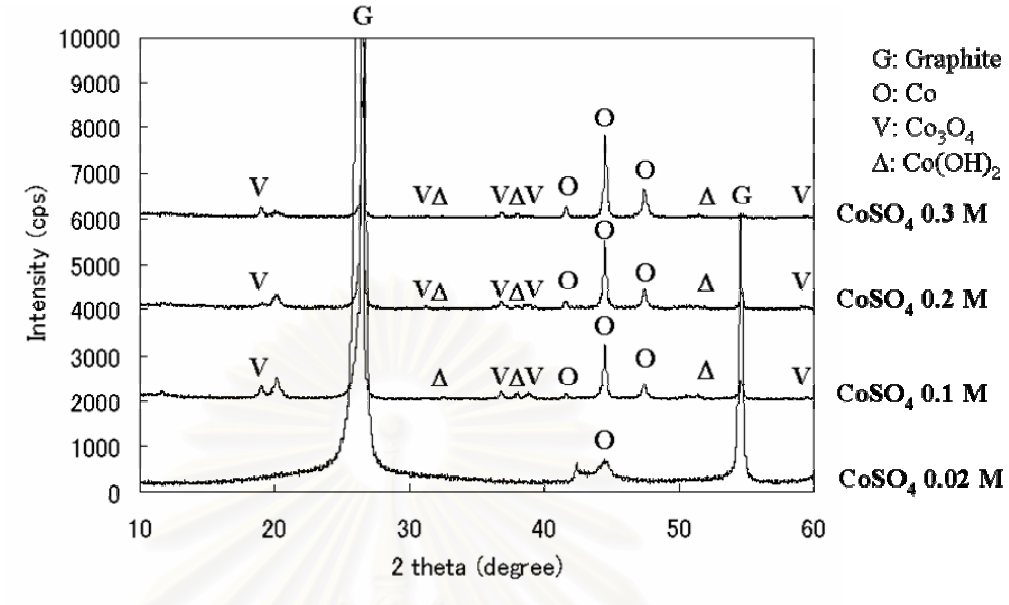

Figure 5.45 XRD patterns obtained from arc in $CoSO_4$ solution

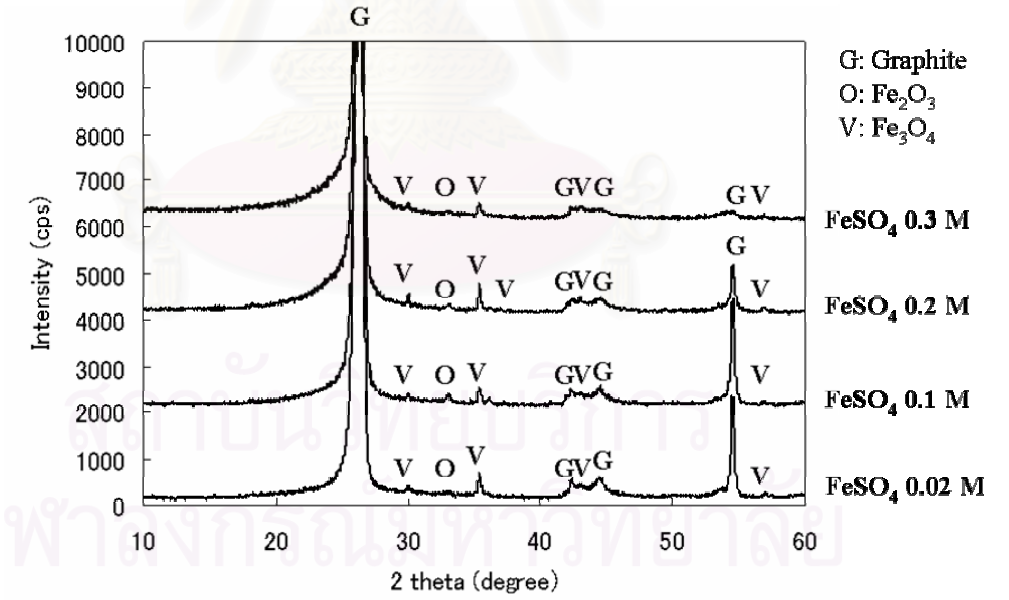

Figure 5.46 XRD patterns obtained from arc in $FeSO_4$ solution

With employing $FeSO_4$, Figure 5.46 presents all conditions could be found the species of iron oxides such as Fe_2O_3 (Hematite) and Fe_3O_4

(Magnetite). It can be concluded that concentration of $FeSO_4$ does not have effect on the formation of iron oxide which are different from two previous cases.

5.2.2.5 Energy Dispersive X-ray pattern (EDX)

The EDX pattern used for analysis the types of elements by shooting the X-ray to the target and then analyzing the released energy from the sample. This released energy depends on the numbers of shell and valence electrons, or it could be said that this released energy depends on the types of elements in the samples. The EDX could be used with the selection of EDX mode in TEM.

The results obtained from EDX pattern by arc in $NiSO_4$ is shown in Figure 5.47. This result is consistent with XRD that NiO can be found in all condition. In this figure, Cu can be also detected because TEM grid which was employed to prepare TEM specimen was made from Cu.

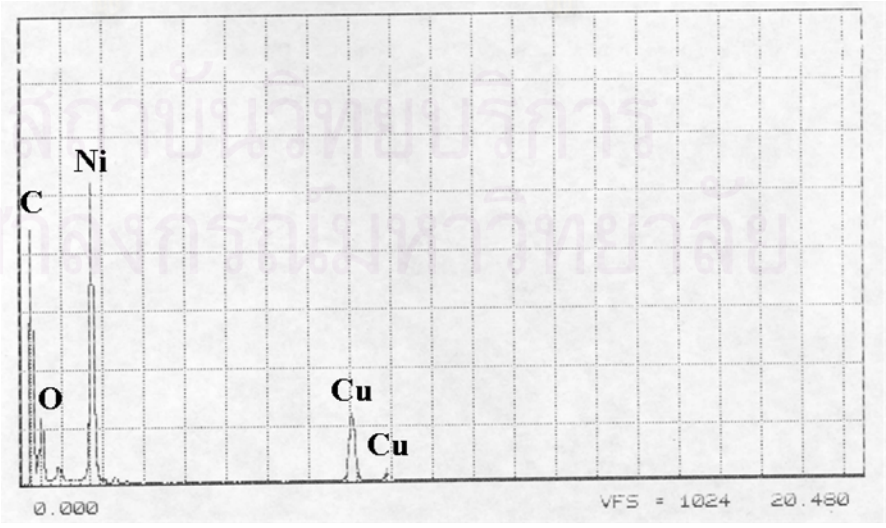

Figure 5.47 EDX pattern of obtained products by arc in $NiSO_4$ solution

Next, in the case of $CoSO_4$, EDX pattern is shown in Figure 5.48. This indicates that Co can be observed in the synthesized product which was consistent with XRD result. Moreover, similar to the $NiSO_4$ case, Cu can be also detected in this graph.

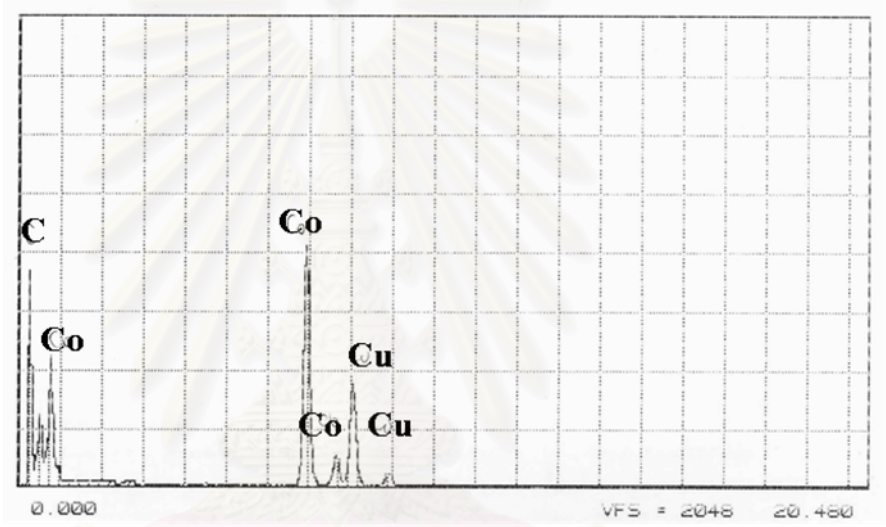

Figure 5.48 EDX pattern of obtained products by arc in $CoSO_4$ solution

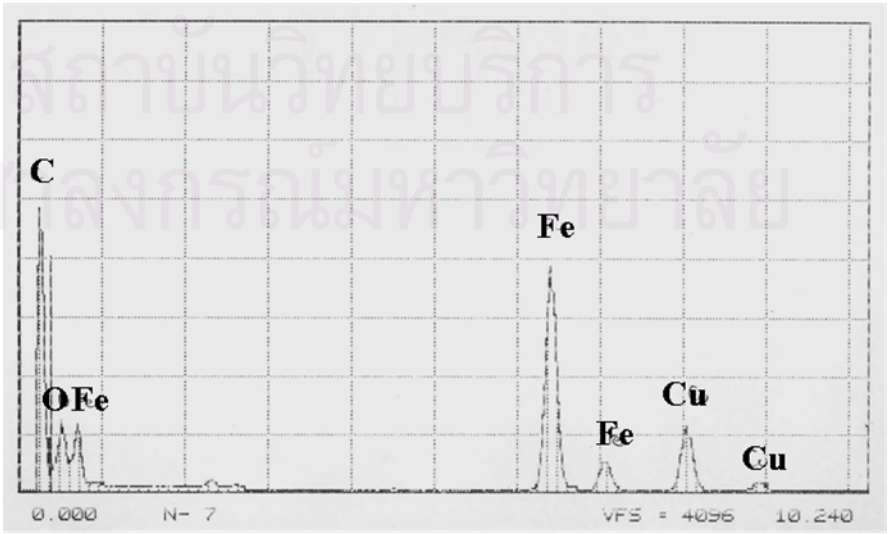

Figure 5.49 EDX pattern of obtained products by arc in $FeSO_4$ solution

In the case of $FeSO_4$, EDX pattern is shown in Figure 5.49. This indicates that iron oxide can be observed in the synthesized product which was consistent with XRD result. Moreover, similar to the two previous case, Cu can be also detected in this graph.

5.2.2.6 Production rate and yield

The production rate of carbon products is also shown in Figure 5.50, it can be seen that there is an optimum point to obtain the highest production rate in each system. The highest production rate for $NiSO_4$, $CoSO_4$ and $FeSO_4$ are approximately 0.05, 0.05, and 0.02 M, respectively.

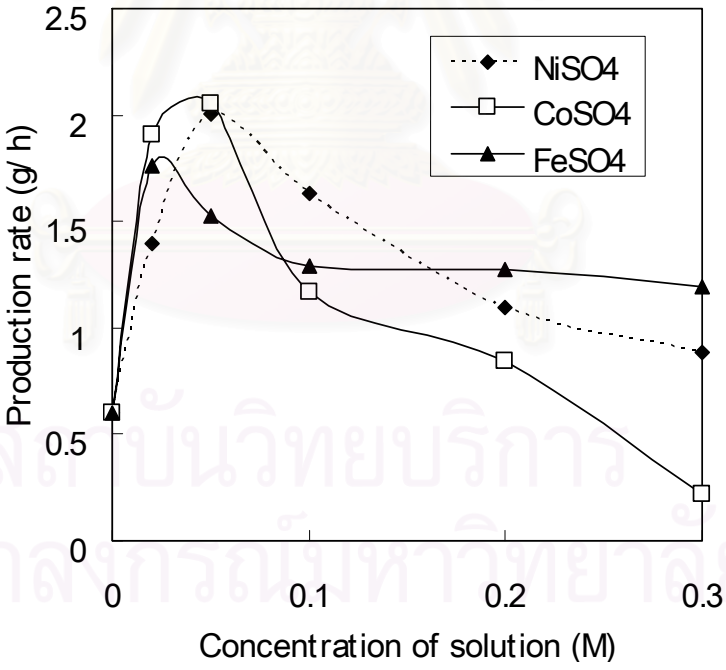

Figure 5.50 Influence of the concentration of solution on the production rate of the carbon products

Yield of the carbon products is also shown in Figure 5.51. This figure indicates that in the case of $NiSO_4$, yield seemed independence from the concentration of solution. With using $CoSO_4$ system, there is an optimum yield at when 0.03 M of $CoSO_4$ solution was utilized. After this point, yield becomes lower with the increasing concentration. When $FeSO_4$ solution was employed, yield change into higher with the increasing concentration of $FeSO_4$.

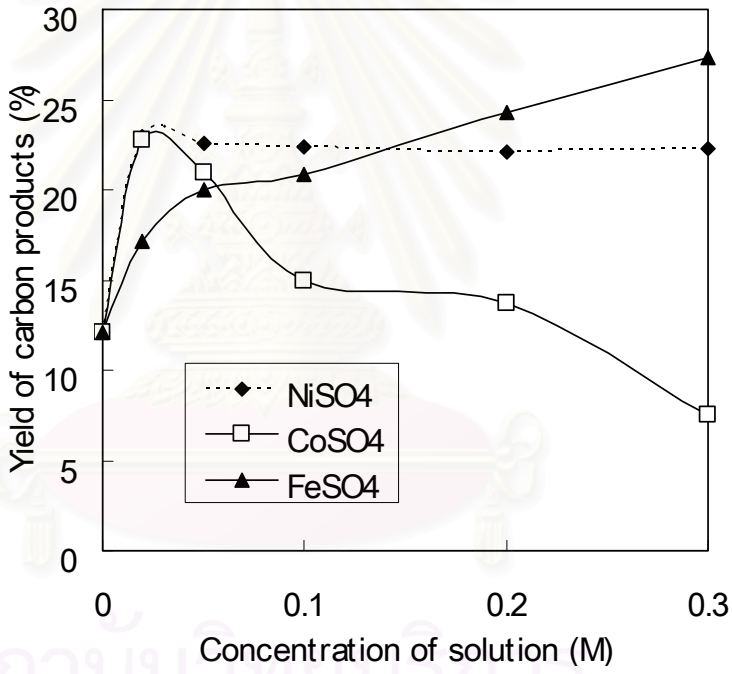

Figure 5.51 Influence of the concentration of solution on the yield percentage of the carbon products

5.2.2.7 Particle size distribution

Typical average particle sizes obtained by DLS are shown in Figure 5.52 as a function of concentration of solution. It could be clearly seen from this figure that both $NiSO_4$ and $CoSO_4$ cases, DLS peak diameter become

higher with the increasing concentration. This is because an increase of concentration, the more metal compound would be obtained in the sample which their particle sizes are broader than CNPs. For the case of $FeSO_4$, the concentration of $FeSO_4$ does not have effect on the particle size of the synthesized product.

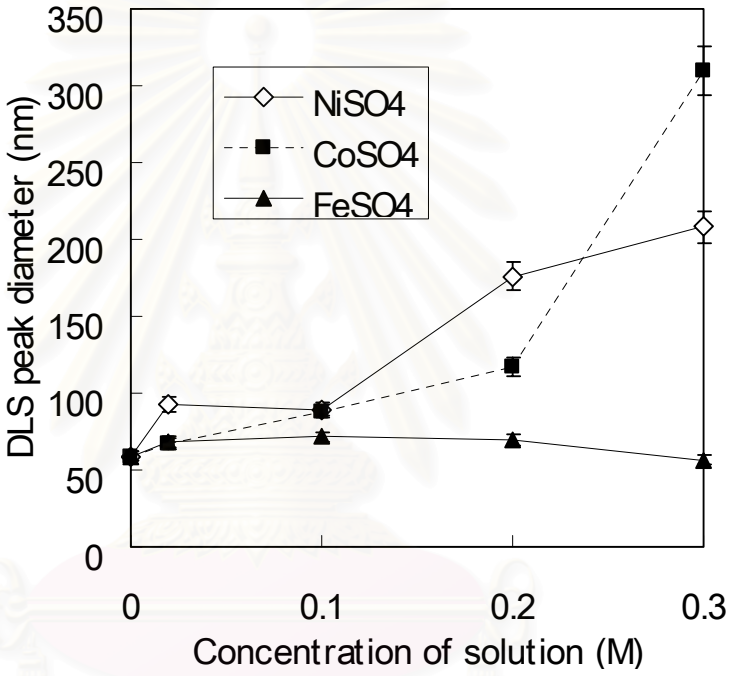

Figure 5.52 Influence of the concentration of solution on the hydrodynamic diameter of obtained products

5.2.2.8 Raman spectroscopic analysis

The G/D ratio of obtained products calculated from Raman spectra are shown in Figure 5.53. It could be clearly seen that when a few amount of metal was employed, these metals would play a role as catalyst to enhance formation of CNPs. Above this point, G/D ratio becomes lower with the increasing concentration of solution because there are some contaminant from

metal compound contained in the obtained products. Based on this result, the appropriate catalyst to enhance the production yield is $FeSO_4$, $CoSO_4$ and $NiSO_4$, respectively due to obtained G/D ratio when 0.03 M of concentration was employed.

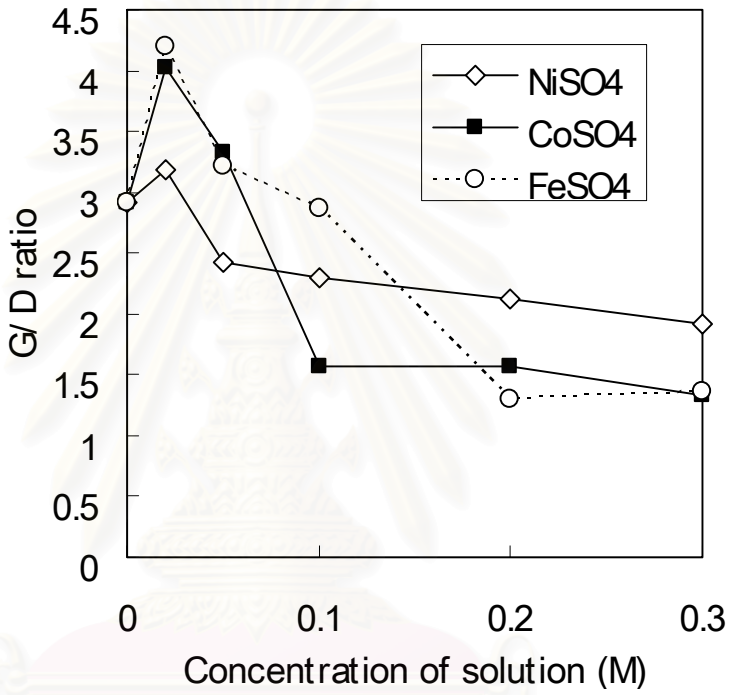

Figure 5.53 Influence of the concentration of solution on the G/D ratio of the obtained products

CHAPTER VI

CONCLUSION AND FUTURE WORKS

6.1 Conclusion

6.1.1 Influence of organic compound

6.1.1.1 Influence of molar ratio in H_2O-C_2H_5OH and H_2O-CH_3OH mixtures

- The CNPs consists of multi-walled carbon nanotubes (MW-CNTs) and multi-shelled carbon nanoparticles were synthesized at higher concentration than that from water in the hard deposit at the cathode tip.
- Arc plasma becomes more stable with an increase in the concentration of alcohol.
- The electrode deposit products become higher while bottom product becomes lower with the increasing of concentration of alcohol.
- Alcohol would play a role of carbon source to produce CNPs in addition to graphite electrodes.
- Average sizes become higher than that from water system.
- Evaporation rate of liquid increase with an increase in concentration of alcohol.

- Some organic byproducts are formed in the residual liquid when alcohol was employed as well as their quantities become higher with the increasing concentration of alcohol.

6.1.1.2 Influence of number of C atoms in n-alcohol ($C_mH_{2m+1}OH$, m=1-8)

- Three types of products can be observed: cathode deposit, sedimentary particle, and anode deposit.
- Arc plasma is very stable in every conditions.
- Purity of CNPs in cathode deposit is about 60-70% based on scanning observation.
- Various organic byproducts are generated in the residual liquid while their types and amounts depend on the carbon numbers in alcohol molecules.
- Average hydrodynamic diameter of CNPs-rich products becomes higher with the increasing carbon numbers in molecule of the liquid media.
- Alcohol would play a role of carbon source to produce CNPs in addition to graphite electrodes which have approximately 8-100 times higher CNPs-rich yield than conventional arc in water.
- Evaporation rate of liquid become lower with an increase in carbon number in alcohol molecules.

6.1.1.3 Influence of number of C atoms in n-alkanes (C_mH_{2m+2}, m=6-7)

- Three types of products can be observed: cathode tip, sedimentary particle, and anode deposit similar to alcohol cases.
- Purity of CNPs in cathode deposit is about 50-60% based on scanning observation.
- Various organic byproducts are synthesized in the residual liquid which is different from alcohol system.
- Average hydrodynamic diameter of CNPs-rich products is higher than that from water system.

6.1.1.4 Influence of aromatic liquid (C_6H_6-C_nH_{2n}, n=1,2)

- Three types of products can be observed: cathode tip, sedimentary particle, and anode deposit.
- Arc plasma is not stable like alcohol and alkane cases.
- Purity of CNPs in cathode tip for aromatic systems becomes lower than 30%.
- CNTs which produced from arc in organic liquid use carbon atoms only from alkyl groups as carbon source.

6.1.1.5 Influence of addition of surfactant (Monoolein)

- There is an optimum point to obtain highest yield and production rate ranging in 0.01-0.1 g of monoolein.
- Purity of CNPs with using surfactant system becomes higher than that from pure water system.
- By using monoolein to prepare the organic liquid-water mixture to accommodate the arc, n-hexane of which vapor

pressure is 1,500-10,000 times lower than pure n-hexane compound could be obtained. This is an effectively alternative method to provide more carbon atoms for reaction which could provide higher safety than using pure organic liquid.

6.1.2 Influence of inorganic liquid

6.1.2.1 Influence of Na_2CO_3 solution

- Arc plasma becomes less stable when increasing the concentration of Na_2CO_3.
- Both yield and production rate decrease with an increase in concentration of Na_2CO_3.
- The maximum concentration at which arc plasma could be maintained is approximately 2.09 M.
- Average hydrodynamic diameter of CNPs from Na_2CO_3 system is higher than that from water system.

6.1.2.2 Influence of transition metal salt solution ($NiSO_4$, $CoSO_4$ and $FeSO_4$)

- An existing of ions in reaction zone only a little amount would play a role as catalyst to enhance formation of CNPs.
- High concentration of CNPs which consist of MWCNTs and polyhedral particles could be obtained in cathode tip.
- Metallic byproducts in various shapes could be synthesized when transition metal salt solutions were employed.

- The percentage of transition metal in the sample becomes higher with the increasing of concentration of solution while arc stability tends to be unstable.
- Species of metallic byproducts with various shapes such as needle and spherical shape could be synthesized depend on the concentration of solution when $NiSO_4$ and $CoSO_4$ were employed.
- There are the optimum condition to obtain highest yield and well crystallinity in ranging between 0.01-0.05 M in each condition.
- The average sizes of CNPs-rich product become higher with an increase of concentration of solution.

6.2 Future Works

- Estimating the arcing temperature at the reaction field when organic compounds were utilized.
- Scaling-up the arc discharge apparatus for using in mass-production.
- Using of sugar solution to supply carbon atoms as a liquid media to accommodate arc plasma.
- Analyzing the species of byproducts existing in residual liquid when organic components were employed.

REFERENCES

[1] M. Terrones. Carbon nanotubes: synthesis and properties, electronic devices and other emerging applications. International Materials Reviews 49, 6 (2004): 325-377.

[2] Sano N., Wang H., Alexandron I., Chhowalla M., Teo K.B.K., Amaratunga G.A.J., and Iimura, K. Properties of carbon onions produced by an arc discharge in water. J. App. Phys. 92, 5 (2002): 2783-2788.

[3] Sano N., Naito M., Chhowalla M., Kikuchi T., Matsuda S., Iimura K., Wang H., Kanki T., and Amaratunga, G.A.J. Pressure effects on nanotubes formation using the submerged arc in water method. Chem. Phys. Lett. 378 (2003): 29-34.

[4] Sano N., Charinpanitkul T., Kanki T., and Tanthapanichakoon, W. Controlled synthesis of carbon nanoparticles by arc in water method with forced convective jet. J. Appl. Phys. 96 (2004): 645-649.

[5] Zhu H.W., Li X.S., Jiang B., Xu C.L., Zhu Y.F., Wu D.H., and Chen, X.H. Formation of carbon nanotubes in water by the electric-arc technique. Chem. Phys. Lett. 366 (2002): 664-669.

[6] Sano N., Wang H., Chhowalla M., Alexandrou I., Amaratunga G.A.J., Naito M., and Kanki, T. Fabrication of inorganic molybdenum disulfide fullerenes by arc in water. Chem. Phys. Lett. 368 (2003): 331-337.

[7] Li X., Zhu H., Jiang B., Ding J., Xu C., Wu, D. High-yield synthesis of multi-walled carbon nanotubes by water-protected arc discharge method. Letter to the editor/ Carbon 411 (2002): 1664-1666.

[8] Cui S., Scharff P., Siegmund C., Spiess L., Romanus H., Schawohl J., Risch K., Schneider D., and Klotzer, S. Preparation of multiwalled carbon nanotubes by DC arc discharge under a nitrogen atmosphere. Letter to the editor/ Carbon 411 (2002): 1645-1687.

[9] Lange H., Sioda M., Huczko A., Zhu Y.Q., Kroto H.W., and Walton, D.R.M. Nanocarbon production by arc discharge in water. Carbon 41 (2003): 1617-1623.

[10] Antisari M. V., Marazzi R., and Krsmanovic, R. Synthesis of multiwall carbon nanotubes by electric arc discharge in liquid environments. Carbon 41 (2003): 2393-2401.

[11] Biro L. P., Horvarth Z. E., Szalmas L., Kertesz K., Weber F., Juhasz G., Radnoczi G., and Gyulai, J. Continuous carbon nanotube production in underwater AC electric arc. Chem. Phys. Lett. 372 (2003): 399-402.

[12] Sano N. Formation of multi-shelled carbon nanoparticles by arc discharge in liquid benzene. Mat. Chem. Phys. 88 (2004): 235-238.

[13] Sano N. Low-cost synthesis of single-walled carbon nanohorns using the arc in water method with gas injection. J. Phys. D: Appl. Phys. 37 (2004): 17-20.

[14] Sano N., Nakano J., and Kanki, T. Synthesis of single-wall carbon nanotubes and nanohorns by arc in liquid nitrogen. Letters to the editor/ Carbon 42 (2004): 667-691.

[15] Sano N. Separated syntheses of Gd-hybridized single-walled carbon nanohorns, single-wall nanotubes and multi-wall nanostructures by arc

discharge in water with support of gas injection. Letters to the editor/ Carbon 43 (2005): 447-453.

[16] Montoro L. A., Lofrano R. C. Z., and Rosolen, J. M. Synthesis of single-walled and multi-walled carbon nanotubes by arc-water method. Letters to the editor/ Carbon 43 (2005): 195-213.

[17] Beck M.T., Dinya Z., and Keki, S. Formation of polycyclic aromatic compounds upon electric discharges in liquid toluene. Tetrahedron 48, 23 (1992): 4919-4928.

[18] Beck M.T., Dinya Z., Keki S., and Papp, L. Formation of C_{60} and polycyclic aromatic hydrocarbons upon electric discharges in liquid toluene. Tetrahedron 49, 1 (1993): 285-290.

[19] Zhao X., Ohkohchi M., Wang M., Iijima S., Ichihashi T. and Ando, Y. Preparation of high-grade carbon nanotubes by hydrogen arc discharge. Carbon 35, 6 (1997): 775-781.

[20] Zeng H., Zhu L., Hao G., and Sheng, R. Synthesis of various forms of carbon nanotubes by AC arc discharge. Carbon 36, 3 (1998): 259-261.

[21] Hutchison J.L., Kiselev N. A., Krinichnaya E. P., Krestinin A. V., Loutfy R. O., Morawsky A. P., Muradyan V. E., Obraztsova E. D., Sloan J., Terekhov S. V., and Zakharov, D. N. Double-walled carbon nanotubes fabricated by a hydrogen arc discharge method. Carbon 39 (2001): 761-770.

[22] Cadek M., Murphy R., McCarthy B., Drury A., Lahr B., Barklie R. C., in het Panhuis M., Coleman J. N., and Blau, W. J. Optimisation of the arc-

discharge production of multi-walled carbon nanotubes. Carbon 40 (2002): 923-928.

[23] Wang Y., Zhang Z., Liu H., Xu X., Pan G., Guo Z., Liu Y., Han X., and Lan, G. The effect of catalyst concentration on the synthesis of single-wall carbon nanotubes. Spectrochimica Acta Part A 58 (2002): 2089-2095.

[24] Ando Y., Zhao X., Inoue S., and Iijima, S. Mass production of multiwalled carbon nanotubes by hydrogen arc discharge. Journal of Crystal Growth 237-239 (2002): 1926-1930.

[25] Nishio M., Akita S., and Nakayama, Y. Cooling effect on the growth of carbon nanotubes and optical emission spectroscopy in short-period arc-discharge. Thin Solid Films 464-465 (2004): 304-307.

[26] Ando Y., Zhao X., Shimoyama H., Sakai G., and Kaneto, K. Physical properties of multiwalled carbon nanotubes. International Journal of Inorganic Materials 1 (1999): 77-82.

[27] Zhao X., Ando Y., Qin L. C., Kataura H., Maniwa Y., and Saito, R. Characteristic Raman spectra of multiwalled carbon nanotubes. Physica B 323 (2002): 265-266.

[28] http://www.sussex.ac.uk/.../ images/c60a.gif.

[29] http://students.chem.tue.nl/ ifp03/default.htm.

[29] Harris P. J. F. Carbon nanotubes and related structures. United Kingdom: Cambridge University Press, 1999.

[30] http://www.itri.org.tw/.../ materials_chem/XD92-05.jsp.

[31] http://www.labs.nec.co.jp/Eng/Topics/data/r010830/.

[32] http://www.arc.eee.tut.ac.jp/.../ pics/Nanohorn_01.jpg.

[33] Cataldo. F. Synthesis of polyynes in a submerged electric arc in organic solvents. Carbon 42 (2004): 129-142.

[34] Hata K., Futaba D. N., Mizuno K., Namai T., Yumura M., Iijima S. Water-Assisted Highly Efficient Synthesis of Impurity-Free Single-Walled Carbon Nanotubes. Science 306 (2004): 1362-1364.

APPENDICES

APPENDIX A

Publication Resulting from This Research Work

PUBLICATIONS

International Proceedings

1. **P. Muthakarn**, T. Charinpanitkul, N. Sano, W. Tanthapanichakoon and T. Kanki, "Production of Carbon Nanoparticles using Submerged Arc in Solution", 12th Joint Seminar between University of Hyogo and Dong-A University, p.6-11, June 4, 2004, Hyogo, JAPAN
2. T. Charinpanitkul, **P. Muthakarn**, N. Sano, W. Tanthapanichakoon and T. Kanki, "Effect of Aqueous Ion Species on Carbon Nanoparticles Synthesis using Arc Discharge in Water Method", 10th The Asian Pacific Confederation of Chemical Engineering (APCChE) Congress, 2004, Kitakyushu, JAPAN
3. **P. Muthakarn**, N. Sano, T. Charinpanitkul and W. Tanthapanichakoon, "Effects of Organic Liquid Components on Carbon Nanoparticles Synthesis Using Arc Discharge in Liquid Method", International Symposium on Nanocarbons (INSC) 2004, p.92, Nagano, JAPAN
4. T. Charinpanitkul, N. Sano, P. Puengjinda, **P. Muthakarn**, T. Kanki, and W. Tanthapanichakoon "Synthesis of carbon nanoparticles using thermal co-pyrolysis of ferrocene and naphthalene mixture", The international conference on smart materials (2004), p.188, Chiang Mai, THAILAND
5. **P. Muthakarn**, N. Sano, W. Tanthapanichakoon, and T. Charinpanitkul " Influence of organic and inorganic additives on carbon nanoparticles formation using arc discharge in water method", 70th Chemical Engineering Conference of Japan (2005), Nagoya, JAPAN

VITA

Mr. Poonlasak Muthakarn was born on April 29, 1981 in Bangkok, Thailand. He studied in primary and secondary educations at Samithichot School and Bodindecha (Sing Singhaseni) School, respectively. In 2001, he received the Bachelor Degree of Engineering (Chemical Engineering) from Chulalongkorn University. After that, he continued to study in Master program in Particle Technology and Material Processing (PTMP). During this, he got two awards; one is the most distinguished poster in 1st Annual Conference on Materials Development and Particle technology (MaDParT 2003), another one is the most outstanding of graduated student in year 2003. Furthermore, he also received the AIEJ scholarship as a research student at Himeji Institute of Technology, University of Hyogo, Japan for one year with Assoc. Noriaki Sano and Prof. Tatsuo Kanki. He graduated in 2004 with the thesis entitled “Production of Carbon Nanoparticles using Arc Discharge in Water Method”.